Computing stable hierarchies of fiber bundles

Thorsten Hüls[*]

Department of Mathematics, Bielefeld University

POB 100131, 33501 Bielefeld, Germany

`huels@math.uni-bielefeld.de`

December 8, 2016

Abstract

Stable fiber bundles are important structures for understanding nonautonomous dynamics. These sets have a hierarchical structure ranging from stable to strong stable fibers. First, we compute corresponding structures for linear systems and prove an error estimate. The spectral concept of choice is the Sacker-Sell spectrum that is based on exponential dichotomies. Secondly, we tackle the nonlinear case and propose an algorithm for the numerical approximation of stable hierarchies in nonautonomous difference equations. This method generalizes the contour algorithm for computing stable fibers from [38, 39]. It is based on Hadamard's graph transform and approximates fibers of the hierarchy by zero-contours of specific operators. We calculate fiber bundles and illustrate errors involved for several examples, including a nonautonomous Lorenz model.

Keywords: Hierarchy of invariant fiber bundles, dynamical systems, noninvertible and nonautonomous dynamics, numerical approximation, contour algorithm.
AMS Subject Classification: 37B55, 37D10, 65P40.

1   Introduction

Invariant manifolds in dynamical systems partition the state space into different areas of attraction. They are of great dynamical relevance in various applications like mathematical biology or chaos theory and we refer to [53, Section 1.1] for further applications. Existence results for invariant manifolds of hyperbolic fixed points in autonomous dynamical systems are given, e.g., in [28, 34, 45, 51] and corresponding results for nonautonomous fiber bundles of bounded trajectories have been developed in [2, 4].

Finding invariant manifolds analytically is hardly possible for many relevant models and numerical approximations are the only feasible alternatives. The

---

literature in this area is quite vast. Proposed techniques are based on numerical continuation, boundary value problems, Taylor expansions, the parameterization method, fixed point iterations and set oriented methods, see [8, 10, 17, 20, 22, 23, 32, 42, 49, 52], where this list is by no means complete. Some of these methods allow nonautonomous generalizations, e.g. [9, 11, 27, 48, 49], but the literature in this area is quite sparse. Finally, we mention techniques for rigorously computing normally hyperbolic manifolds and for proving their existence, see [12, 13, 24].

The problem gets more involved when asking for hierarchies of invariant manifolds, see [51, Chapter 5]. The stable hierarchy ranges from the stable to the strong stable manifold and provides information on regions within the stable manifold, having different rates of attraction.

We even go one step further and aim for computing hierarchies in nonautonomous discrete time systems

$$x_{n+1} = F_n(x_n), \quad F_n \in \mathcal{C}^2(\mathbb{R}^d, \mathbb{R}^d), \quad n \in \mathbb{Z}. \tag{1}$$

The family of maps $(F_n)_{n \in \mathbb{Z}}$ may arise via discrete time modeling or it may result from a discretization of a nonautonomous continuous time system. The reference object for which we define stable hierarchies are bounded trajectories $\xi_{\mathbb{Z}} = (\xi_n)_{n \in \mathbb{Z}}$ of (1). Fixed points that are frequently chosen as reference objects in autonomous systems, typically do not exist in the nonautonomous context.

Fibers from the stable hierarchy can locally be expressed as graphs over the corresponding stable subspace, see [4, Theorem 4.11] and [46, Theorem 4.6.4]. Before we propose an approach for their approximation in Section 3, we specify the precise meaning of a hierarchy of stable subspaces. For this purpose, a linear theory for the so called variational equation

$$u_{n+1} = DF_n(\xi_n)u_n, \quad n \in \mathbb{Z} \tag{2}$$

is introduced in detail in Section 2. If the underlying system is autonomous and $\xi_{\mathbb{Z}}$ is a fixed point, then (2) turns into a linear, autonomous difference equation

$$u_{n+1} = Au_n, \quad A \in \mathbb{R}^{d,d}, \quad n \in \mathbb{Z}. \tag{3}$$

Assuming that A is hyperbolic, i.e. A has no eigenvalue on the unit circle, it follows that eigenvalues with corresponding generalized eigenvectors provide complete information on the underlying dynamics. The analysis changes dramatically, when considering the nonautonomous equation (2) or, more generally

$$u_{n+1} = A_n u_n, \quad A_n \in \mathbb{R}^{d,d}, \quad n \in \mathbb{Z}. \tag{4}$$

This setup requires adequate spectral concepts, since eigenvalues are in general meaningless as shown by Vinograd, cf. [14, Section 2.6]. The Sacker-Sell spectrum, also called dichotomy spectrum provides the desired stability information. Of particular interest are corresponding spectral bundles that are the nonautonomous analog of eigenspaces. We review in Section 2 an algorithm from [25,

Section 3] for computing spectral bundles and recall a precise estimate of the errors involved from [25, Section 3.1]. Its proof that was postponed in [25] to a forthcoming publication is presented here. An example illustrates that this estimate is rather sharp.

After establishing the linear theory, we tackle nonlinear approximations of stable fibers in Section 3. The main tool is the contour algorithm that was proposed in [38, 39]. Note that F_n is not assumed to be invertible. The algorithm is based on Hadamard's graph transform [28], but avoids an infinite fixed point iteration. In the end, the problem reduces to the computation of the zero-contour of some function $f : \mathbb{R}^r \to \mathbb{R}$, where r is the dimension of the stable fiber. For this task, efficient software applies, such as the MATLAB commands `contour` and `isosurface` in cases $r = 2$ and $r = 3$, respectively. This ansatz restricts the space dimension d to $d \in \{2, 3\}$ and requires the unstable fibers to be one-dimensional. Overcoming several of these restrictions constitutes a novelty of this paper. Furthermore, an extension of the contour algorithm is introduced that enables approximating the whole stable hierarchy. Error estimates justify the numerical procedure.

We apply the resulting algorithm to various examples of dimension three and four. In particular, error estimates are verified numerically for models with explicitly given stable hierarchies. Numerical strategies for the computation of hierarchies are illustrated in case of non-global graph representations. Finally, we determine the stable hierarchy for a nonautonomous variant of the famous Lorenz system [43].

2 Computation of spectral bundles for linear systems

Spectral bundles in nonautonomous linear systems (4) are the analog of eigenspaces in autonomous systems. We review an algorithm from [25] for their numerical approximation and analyze occurring errors. Finally, we illustrate that the derived rates of convergence are rather sharp.

We start with the introduction of our basic notion of hyperbolicity – the so called exponential dichotomy.

2.1 Exponential dichotomy

The solution operator Φ of the difference equation (4) is given by

$$\Phi(n, m) = \begin{cases} A_{n-1} \cdot \ldots \cdot A_m, & \text{for } n > m, \\ I, & \text{for } n = m. \end{cases}$$

Let $P_{\mathbb{Z}}^{s,u}$ be two families of complementary, invariant projectors, i.e.

$$P_n^u = I - P_n^s, \quad P_n^{s,u}\Phi(n, m) = \Phi(n, m)P_m^{s,u} \quad \text{for all} \quad n, m \in \mathbb{Z}, \ n \geq m. \quad (5)$$

3

Denote by $\mathcal{R}(P)$ the range of a projector P. If the operator

$$\Phi(n,m)_{|\mathcal{R}(P_m^u)} : \mathcal{R}(P_m^u) \to \mathcal{R}(P_n^u), \quad n \geq m$$

is invertible, then the same symbol $\Phi(m,n) : \mathcal{R}(P_n^u) \to \mathcal{R}(P_m^u)$ is used for its inverse.

We define the notion of an exponential dichotomy, following the references [33, Definition 7.6.1] and [3, Definition 3.1], [41]. For the development of this important notion of hyperbolicity, we refer to [15, 16, 44].

Definition 1 *The difference equation* (4) *has an **exponential dichotomy (ED** for short) with data* $(K, \alpha_{s,u}, P_{\mathbb{Z}}^{s,u})$ *on* $\mathbb{Z}$, *if there exist constants* $K, \alpha_s, \alpha_u > 0$ *and two families of projectors* $P_{\mathbb{Z}}^{s,u}$ *that satisfy* (5), *such that*

(i) $A_n|_{\mathcal{R}(P_n^u)} : \mathcal{R}(P_n^u) \to \mathcal{R}(P_{n+1}^u)$ *is invertible for all* $n \in \mathbb{Z}$.

(ii) *For* $n, m \in \mathbb{Z}$, $n \geq m$ *the following estimates hold:*

$$\|\Phi(n,m)P_m^s\| \leq K\mathrm{e}^{-\alpha_s(n-m)}, \quad \|\Phi(m,n)P_n^u\| \leq K\mathrm{e}^{-\alpha_u(n-m)}.$$

2.2 Sacker-Sell spectrum

The Sacker-Sell spectrum, cf. [50], also known as dichotomy spectrum, is based on considering the scaled equation

$$u_{n+1} = \frac{1}{\gamma}A_n u_n, \quad n \in \mathbb{Z}. \tag{6}$$

We define the Sacker-Sell spectum $\Sigma_{\mathrm{ED}} := \{\gamma > 0 : (6) \text{ has no ED on } \mathbb{Z}\}$ and the resolvent set $R_{\mathrm{ED}} := \mathbb{R} \setminus \Sigma_{\mathrm{ED}}$. Alternatively, this spectral notion may be derived from operator theory, cf. [47]. For $n \in \mathbb{Z}$ let $(Tu)_n := A_{n-1}u_{n-1}$ and denote by $\Sigma(T)$ the spectrum of this linear operator in suitable spaces of bounded sequences. Then $\Sigma_{\mathrm{ED}} = \Sigma(T) \cap (0, \infty)$.

Assuming that all matrices $A_n \in \mathbb{R}^{d,d}$ are uniformly bounded, it follows from the Spectral Theorem in [5] that Σ_{ED} consists of $\ell \leq d$ intervals of the form

$$\Sigma_{\mathrm{ED}} = \bigcup_{i=1}^{\ell-1}[\sigma_i^-, \sigma_i^+] \cup \mathcal{I}_\ell, \quad \text{where} \quad 0 < \sigma_\ell^+ < \sigma_{\ell-1}^- \leq \sigma_{\ell-1}^+ < \cdots \leq \sigma_1^+$$

with two possible cases for $\mathcal{I}_\ell$. In case 1, $\mathcal{I}_\ell = (0, \sigma_\ell^+]$ and in case 2, $\mathcal{I}_\ell = [\sigma_\ell^-, \sigma_\ell^+]$, where $0 < \sigma_\ell^- \leq \sigma_\ell^+$. As a consequence, the resolvent set reads $R_{\mathrm{ED}} = \bigcup_{i=1}^{\ell+1} R_i$ with

$$R_1 = (\sigma_1^+, \infty), \quad R_i = (\sigma_i^+, \sigma_{i-1}^-), \ i = 2, \ldots, \ell, \quad R_{\ell+1} = \begin{cases} \emptyset, & \text{in case 1,} \\ (0, \sigma_\ell^-), & \text{in case 2,} \end{cases}$$
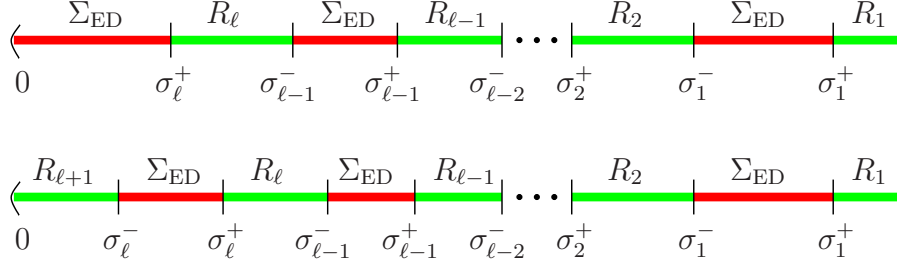
see Figure 1.

Figure 1: Illustration of spectral and resolvent intervals.

Spectral intervals of Σ_{ED} may consist of isolated points, only. The autonomous system (3), for example, has the Sacker-Sell spectrum $\Sigma_{\mathrm{ED}} = \{|\lambda| : \lambda \in \Sigma(A), \lambda \neq 0\}$, where $\Sigma(A)$ denotes the set of eigenvalues of A.

The upper case in Figure 1 may occur, if A_n is noninvertible for some n or if $\sup_{n\in\mathbb{Z}} \|A_n^{-1}\| = \infty$.

Finally, we note that the Sacker-Sell spectrum is closely related to the set of Bohl exponents, see [40, Appendix B.2].

2.3   Spectral bundles

For $i \in \{1, \ldots, \ell + 1\}$ and $\gamma \in R_i$ we denote by $P_{\mathbb{Z},i}^{s,u}$ the dichotomy projectors of the scaled equation (6). Note that dichotomy projectors on $\mathbb{Z}$ are uniquely determined. In particular, dichotomy projectors do not depend in the i-th resolvent interval R_i on the specific value of $\gamma \in R_i$. The regularity condition (i) of Definition 1 guarantees that for all $\gamma \in R_i$, the solution operator $\Phi(\cdot, n)$ is invertible in $\mathcal{R}(P_{n,i}^u)$. Further note that $\mathcal{R}(P_{n,1}^s) = \mathbb{R}^d$ and

$$d_i^s := \dim(\mathcal{R}(P_{n,i}^s)), \quad d_i^u := d - d_i^s, \quad i = 1, \ldots, \ell + 1 \tag{7}$$

are well defined, since the dimension of $\mathcal{R}(P_{n,i}^s)$ does not depend on n. The value of d_i^s is strictly decreasing with respect to i. Dichotomy projectors have a hierarchical structure for $n \in \mathbb{Z}$

$$\{0\} \subset \mathcal{R}(P_{n,\ell+1}^s) \subset \mathcal{R}(P_{n,\ell}^s) \subset \cdots \subset \mathcal{R}(P_{n,1}^s) = \mathbb{R}^d,$$
$$\mathbb{R}^d \supset \mathcal{R}(P_{n,\ell+1}^u) \supset \mathcal{R}(P_{n,\ell}^u) \supset \cdots \supset \mathcal{R}(P_{n,1}^u) = \{0\} \tag{8}$$

and it follows for all $n \in \mathbb{Z}$ and $i = 1, \ldots, \ell$ that

$$P_{n,i+1}^s P_{n,i}^s = P_{n,i+1}^s, \tag{9}$$
$$P_{n,i}^u P_{n,i+1}^s = P_{n,i+1}^s P_{n,i}^u = 0. \tag{10}$$

We introduce the spectral bundles

$$\begin{aligned} \mathcal{W}_n^i &:= \mathcal{R}(P_{n,i}^s) \cap \mathcal{R}(P_{n,i+1}^u), \quad i = 1, \ldots, \ell, \\ \mathcal{W}_n^{\ell+1} &:= \mathcal{R}(P_{n,\ell+1}^s). \end{aligned} \tag{11}$$

For $i = 1, \ldots, \ell$, we note that

$$
\begin{aligned}
\mathcal{W}_n^i = \mathcal{R}(P_{n,i}^s) \cap \mathcal{R}(P_{n,i+1}^u) &= \{x \in \mathbb{R}^d : P_{n,i}^s x = x \text{ and } P_{n,i+1}^s x = 0\} \\
&= \{x \in \mathbb{R}^d : P_{n,i}^s x = x \text{ and } P_{n,i+1}^s P_{n,i}^s x = 0\} \quad (12) \\
&= \{x \in \mathbb{R}^d : P_{n,i+1}^u P_{n,i}^s x = x\} = \mathcal{R}(P_{n,i+1}^u P_{n,i}^s).
\end{aligned}
$$

One observes invariance of spectral bundles, i.e. $\Phi(n,m)\mathcal{W}_m^i = \mathcal{W}_n^i$ for all $n, m \in \mathbb{Z}$ and $i \in \{1, \ldots, \ell+1\}$. For $i \neq j$, it turns out that $\mathcal{W}_n^i \cap \mathcal{W}_n^j = \{0\}$. Furthermore, $\bigoplus_{i=1}^{\ell+1} \mathcal{W}_n^i = \mathbb{R}^d$ holds true.

If all matrices A_n from (4) are invertible, and A_n, A_n^{-1} are uniformly bounded, then the resolvent interval $R_{\ell+1}$ is nonempty. In this case, the $\ell + 1$-th spectral bundle turns out to be trivial $\mathcal{W}_n^{\ell+1} = \mathcal{R}(P_{n,\ell+1}^s) = \{0\}$.

An example with nontrivial spectral bundle $\mathcal{W}_n^{\ell+1}$ is given by (3) with $A = \left(\begin{smallmatrix} 0 & 0 \\ 0 & 2 \end{smallmatrix} \right)$. In this example, $\ell = 1$ and we obtain $\mathcal{W}_n^{\ell+1} = \mathcal{R}(P_{n,2}^s) = \text{span}\{\left(\begin{smallmatrix} 1 \\ 0 \end{smallmatrix} \right)\}$.

2.4 Spectral bundles and Lyapunov transformations

It is well known that the Sacker-Sell spectrum is invariant w.r.t. a Lyapunov transformation of the equation, i.e. the Sacker-Sell spectrum of (4) coincides with the spectrum of

$$
u_{n+1} = S_{n+1}^{-1} A_n S_n u_n, \quad n \in \mathbb{Z}, \quad (13)
$$

where $S_n \in \mathbb{R}^{d,d}$, $n \in \mathbb{Z}$ are invertible, and both S_n and S_n^{-1} are uniformly bounded. Corresponding dichotomy projectors are given by $S_n^{-1} P_{n,i}^{s,u} S_n$ and consequently, spectral bundles $\tilde{\mathcal{W}}_n^i$ of (13) satisfy

$$
\tilde{\mathcal{W}}_n^i = S_n^{-1} \mathcal{W}_n^i \quad \text{for} \quad i = 1, \ldots, \ell+1 \text{ and } n \in \mathbb{Z}. \quad (14)
$$

Two systems (4) and (13) that are conjugate via a Lyapunov transformation are called kinematically similar.

2.5 An algorithm for computing spectral bundles

In the following, we denote by $J = [n_-, n_+] \cap \mathbb{Z}$ and $\tilde{J} = [n_-, n_+ - 1] \cap \mathbb{Z}$ finite discrete intervals. Our approach for the approximation of spectral bundles $\mathcal{W}_n^i$ is based on techniques for the calculation of dichotomy projectors from [35, Section 2] and [36, Section 2] and on the observation that $\mathcal{W}_n^i = \mathcal{R}(P_{n,i}^s P_{n,i+1}^u)$ for $i = 1, \ldots, \ell$, see (12). The algorithm proposed in [25, Section 3] allows the computation of $\bar{w} = P_{N,i}^s P_{N,i+1}^u r$ for a given vector $r \in \mathbb{R}^d$ along the following steps:

Setup: Fix $i \in \{1, \ldots, \ell\}$, $r \in \mathbb{R}^d$, $N \in \mathbb{Z}$, $\gamma_i \in R_i$, $\gamma_{i+1} \in R_{i+1}$ and $n_- \ll N \ll n_+$.

Approximation of $x = P^u_{N,i+1} r$: Compute the least squares solution of

$$v_{n+1} = \tfrac{1}{\gamma_{i+1}} A_n v_n + \delta_{n,N-1} r, \quad n \in \tilde{J}, \tag{15}$$

where δ denotes the Kronecker symbol. Define

$$x := -A_{N-1} v_{N-1}. \tag{16}$$

Approximation of $w = P^s_{N,i} x$: Compute the least squares solution of

$$u_{n+1} = \tfrac{1}{\gamma_i} A_n u_n + \delta_{n,N-1} x, \quad n \in \tilde{J} \tag{17}$$

and define

$$w := u_N.$$

2.6 Error estimates

By calculating the unique bounded solutions of (15) and (17) on $\mathbb{Z}$, we obtain the vector $\bar{w} \in \mathcal{W}^i_N$. In practice, we are forced to solve (15), (17) on finite intervals and numerical errors cannot be avoided. We prove that errors decays exponentially fast by increasing the length of the finite interval J. Furthermore, our estimates indicate optimal choices of γ_i and γ_{i+1} inside corresponding resolvent intervals.

Our main interest is to accurately approximate the subspace $\mathcal{W}^i_N$ rather than the particular vector $\bar{w} \in \mathcal{W}^i_N$. Thus, approximation errors within $\mathcal{W}^i_N$ are irrelevant and it suffices to discuss the relevant error

$$
\begin{aligned}
d_{N,i} &:= [I - P^s_{N,i} P^u_{N,i+1}] u_N \\
&= [I - (I - P^u_{N,i})(I - P^s_{N,i+1})] u_N = [P^s_{N,i+1} + P^u_{N,i}] u_N,
\end{aligned} \tag{18}
$$

see (10).

Theorem 2 *Fix $r \in \mathbb{R}^d$, $N \in \mathbb{Z}$, $i \in \{1, \ldots, \ell\}$ and $\gamma_j \in R_j$ for $j \in \{i, i+1\}$. Denote by $(K, \alpha^{s,u}_j, P^{s,u}_{\mathbb{Z},j})$ the corresponding dichotomy data of the scaled equation (6). Let $J = [n_-, n_+]$ with $N \in J$. Then the relevant error $d_{N,i}$ of the least squares approximation $w = u_N$ of (15), (17) satisfies the inequality*

$$\|d_{N,i}\| \leq C \left(e^{-\alpha^s_{i+1}(N-n_-)} + e^{-\alpha^u_i(n_+-N)} \right) \tag{19}$$

with some constant C that does not depend on $n_\pm$.

Proof: Denote by Φ_j the solution operator of (6) with $\gamma = \gamma_j$, $j \in \{i, i+1\}$. Let $\bar{u}_{\mathbb{Z}}$ be the unique bounded solution on $\mathbb{Z}$ of (17). Here, x is defined in (16), using the least squares solution v_J of (15) w.r.t. the finite interval J. It follows that

$$d_{N,i} = d^1_{N,i} + d^2_{N,i} + d^3_{N,i},$$

7

where

$$d_{N,i}^1 = (P_{N,i+1}^s + P_{N,i}^u)\bar{u}_N, \quad d_{N,i}^2 = P_{N,i}^u(u_N - \bar{u}_N), \quad d_{N,i}^3 = P_{N,i+1}^s(u_N - \bar{u}_N).$$

We derive estimates for the three terms, starting with $d_{N,i}^1$.

The unique bounded solution of (17) on $\mathbb{Z}$ is given by $\bar{u}_N = P_{N,i}^s x$, see [36, Theorem 2]. Thus, we conclude using (9), (16) that

$$d_{N,i}^1 = P_{N,i+1}^s P_{N,i}^s x + P_{N,i}^u P_{N,i}^s x = P_{N,i+1}^s x = -P_{N,i+1}^s A_{N-1} v_{N-1}, \qquad (20)$$

with least squares solution v_J from (15). The vector v_{N-1} can be decomposed as follows

$$\begin{aligned}
v_{N-1} &= -\Phi_{i+1}(N-1,N)P_{N,i+1}^u r + \Phi_{i+1}(N-1,n_-)P_{n_-,i+1}^s \eta_v(n_\pm) \\
&\quad + \Phi_{i+1}(N-1,n_+)P_{n_+,i+1}^u \xi_v(n_\pm),
\end{aligned} \qquad (21)$$

where η_v and ξ_v are uniformly bounded by some constant $L > 0$ due to [35, Theorem 4.1]. Indeed, η_v and ξ_v decay exponentially fast to 0 as $n_\pm \to \pm\infty$. Inserting (21) into (20), one gets $d_{N,i}^1 = -\Phi_{i+1}(N,n_-)P_{n_-,i+1}^s \eta_v(n_\pm)$ and thus

$$\|d_{N,i}^1\| \le L\|\Phi_{i+1}(N,n_-)P_{n_-,i+1}^s\| \le LKe^{-\alpha_{i+1}^s(N-n_-)}.$$

For an estimate of the remaining terms, we observe from [35, Theorem 4.1] the similar decomposition

$$u_N - \bar{u}_N = \Phi_i(N,n_-)P_{n_-,i}^s \eta_u(n_\pm) + \Phi_i(N,n_+)P_{n_+,i}^u \xi_u(n_\pm), \qquad (22)$$

where $\|\eta_u\|, \|\xi_u\| \le L$. We conclude that

$$\|d_{N,i}^2\| = \|P_{N,i}^u(u_N - \bar{u}_N)\| \le \|\Phi_i(N,n_+)P_{n_+,i}^u\|\|\xi_u(n_\pm)\| \le LKe^{-\alpha_i^u(n_+-N)}.$$

Finally, one obtains from (9), (10), (22) and

$$\Phi_i(N,n_-) = \left(\tfrac{\gamma_{i+1}}{\gamma_i}\right)^{N-n_-}\Phi_{i+1}(N,n_-) \quad \text{with} \quad \gamma_{i+1} < \gamma_i$$

the estimate

$$\begin{aligned}
\|d_{N,i}^3\| &\le \|P_{N,i+1}^s \Phi_i(N,n_-)P_{n_-,i}^s \eta_u(n_\pm)\| \le \|\Phi_i(N,n_-)P_{n_-,i+1}^s\|\|\eta_u(n_\pm)\| \\
&\le L\|\Phi_{i+1}(N,n_-)P_{n_-,i+1}^s\| \le LKe^{-\alpha_{i+1}^s(N-n_-)}.
\end{aligned}$$

Combining the three estimates, the proof of (19) with $C = 3KL$ is complete. ∎

It follows from

$$\Phi_j(n,m) = \left(\tfrac{1}{\gamma_j}\right)^{n-m}\Phi(n,m), \quad j \in \{1,\dots,\ell+1\} \qquad (23)$$

that the stable dichotomy rate α_{i+1}^s is maximal, if γ_{i+1} is chosen close to the right boundary of the resolvent interval R_{i+1}. On the other hand, a choice of γ_i close

8

to the left boundary of R_i results in a maximal unstable rate α_i^u. Pushing these values towards the right respectively left boundary of the corresponding resolvent interval, we obtain in the limit the maximal rates

$$\alpha_{i+1}^s = \log \sigma_i^- - \log \sigma_{i+1}^+ = \log \frac{\sigma_i^-}{\sigma_{i+1}^+}, \quad \alpha_i^u = \log \sigma_{i-1}^- - \log \sigma_i^+ = \log \frac{\sigma_{i-1}^-}{\sigma_i^+}, \quad (24)$$

see Figure 2. With these choices, Theorem 2 guarantees optimal rates of convergence of the algorithm from Section 2.5. Using (24), our error estimate (19) reads

$$\|d_{N,i}\| \le C \left(\left(\frac{\sigma_{i+1}^+}{\sigma_i^-} \right)^{N-n_-} + \left(\frac{\sigma_i^+}{\sigma_{i-1}^-} \right)^{n_+ - N} \right). \quad (25)$$

Note that in case $i = 1$ there is no unstable direction and the second term in (25) vanishes in accordance with the formal result $\sigma_0^- = \infty$, from which $\alpha_1^u = \infty$ follows. In case $R_{\ell+1} = (0, \sigma_\ell^-)$, we similarly conclude that $\alpha_{\ell+1}^s = \infty$.
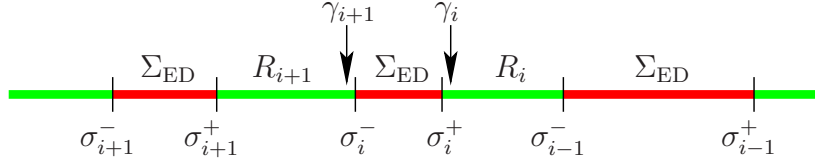

Figure 2: Optimal choices of γ_i and γ_{i+1}.

2.7 A linear example with explicitly given spectral bundles

We apply the algorithm from Section 2.5 to a model, for which spectral bundles are explicitly known. This model is a noninvertible version of [25, Section 5.1]. An inspection of approximation errors particularly illustrates that our estimate (19) is rather sharp.

Fix $d \in \mathbb{N}$ and let $\sigma_i = \frac{2(d-i)}{d-1}$ for $i = 1, \dots, d$. We define the diagonal matrix $B := \operatorname{diag}(\sigma_1, \dots, \sigma_d)$ and arrive at a nonautonomous system (4) via the Lyapunov transformation

$$A_n := S_{n+1}^{-1} B S_n, \quad \text{where} \quad S_n^{-1} = \begin{cases} I, & \text{if } n = 0, \\ I + 0.1 X_n, & \text{otherwise.} \end{cases} \quad (26)$$

Here, $X_{\mathbb{Z}}$ is a sequence of random matrices with independent, uniformly distributed entries in $[0, 1]$.

For this model, $\ell = d - 1$ and the Sacker-Sell spectrum $\Sigma_{ED} = \bigcup_{i=1}^{\ell} \{\sigma_i\}$ consists of isolated point only, see Figure 3.

If follows from (14) that spectral bundles at time $N = 0$ have the explicit representation $\mathcal{W}_0^i = \operatorname{span}\{e_i\}$, $i = 1, \dots d$, where e_i denotes the i-th unit vector in $\mathbb{R}^d$.

We compute fibers $\mathcal{W}_0^i$ by applying the algorithm from Section 2.5. First, one needs an approximation of the Sacker-Sell spectrum in order to set up γ_i and
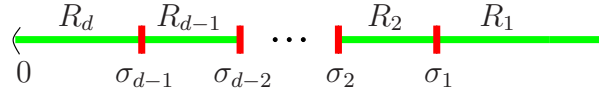
9

Figure 3: Sacker-Sell spectrum and resolvent set of (26).

γ_{i+1} close to the boundaries of corresponding spectral intervals. In this particular example, we use the explicitly given spectrum. Note that various techniques for calculating spectral intervals have been developed. We refer to [18, 19] for SVD- and QR-methods that also apply to discrete time systems. An alternative ansatz that is based on solving boundary value problems was proposed in [36].

Let $\ell = 6$ and choose $\gamma_{i+1} = \sigma_i - \varepsilon$ and $\gamma_i = \sigma_i + \varepsilon$ with $\varepsilon = 0.01$, $i = 1, \ldots, 6$. Next, the dependence of (19) on n_+ is verified numerically. For this task, we fix $n_- = -400$, resulting in exponentially small errors from the left boundary, which can be neglected. Occurring errors $d_{0,i}$, $i = 1, \ldots, 6$, cf. (18), of spectral bundles are computed for $n_+ = 10, \ldots, 100$. Figure 4 illustrates the numerical data. From (19), an error of the form $\|d_{0,i}\| \approx C e^{-\alpha_i^u n_+}$ is expected. We compare the exponential slope of the data in Figure 4 with an estimate of α_i^u that is obtained from the length of the corresponding resolvent interval, see (24). Recall that $\alpha_1^u = \infty$ and consequently, we expect no approximation error when computing $d_{0,1}$. This is confirmed by the numerical experiment in Figure 4.
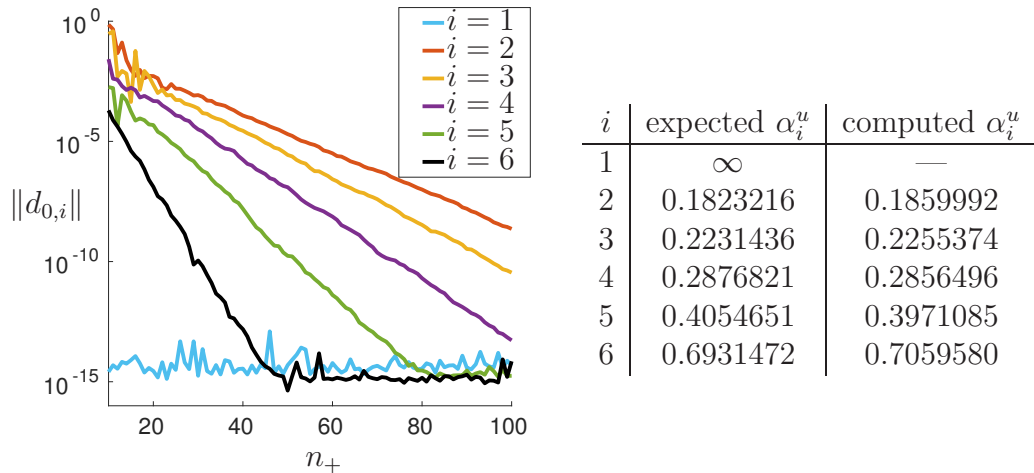

i	expected α_i^u	computed α_i^u
1	∞	—
2	0.1823216	0.1859992
3	0.2231436	0.2255374
4	0.2876821	0.2856496
5	0.4054651	0.3971085
6	0.6931472	0.7059580

Figure 4: Errors of approximate spectral bundles of (26) for $n_- = -400$, $n_+ = 10, \ldots, 100$.

Similarly, we fix $n_+ = 400$ and vary $n_- = -10, \ldots, -100$ to analyze the dependence of (19) on n_-. A comparison of the exponential slope of errors of spectral bundles in Figure 5 with an approximation of α_{i+1}^s supports the estimate $\|d_{0,i}\| \approx C e^{\alpha_{i+1}^s n_-}$, $i = 1, \ldots, 6$. Here, $\alpha_7^s = \infty$ and thus, $\|d_{0,6}\| = 0$ up to machine accuracy.
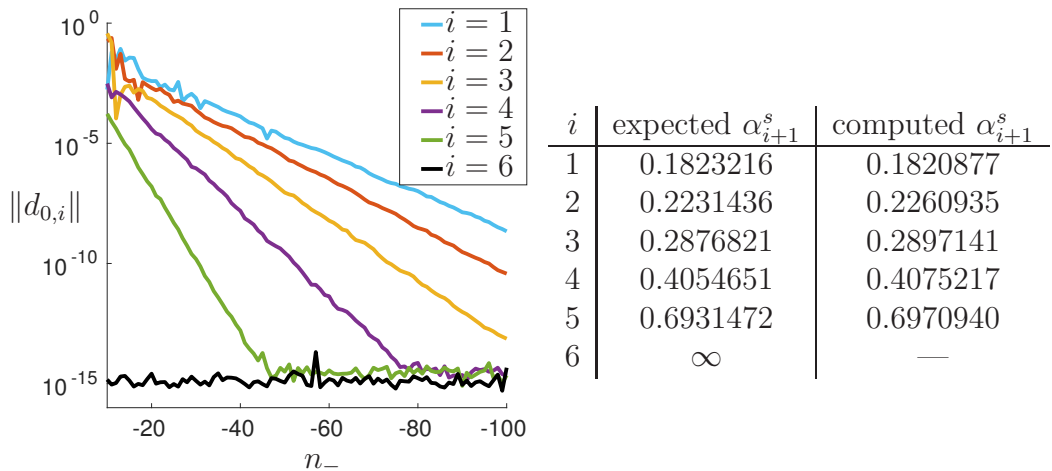
10

Figure 5: Errors of approximate spectral bundles of (26) for $n_+ = 400$, $n_- = -10, \ldots, -100$.

Finally, we note that in [25], the algorithm from Section 2.5 is applied to models from particle dynamics and to time-dependent fluid flows. These models fit into our linear framework, after applying a finite rank approximation of the Perron-Frobenius opearator that tracks the evolution of densities over short time intervals, see [26] for details.

3 Stable hierarchies of fiber bundles for nonlinear systems and their approximation

We now turn our attention to nonautonomous nonlinear systems.

Recall that the linear system (4) has unique dichotomy projectors, when considered on $\mathbb{Z}$. As a consequence, spectral bundles $\mathcal{W}_n^i$ – as defined in Section 2.3 – are uniquely determined.

For the system (1), uniqueness of a nonlinear version of $\mathcal{W}_n^i$ cannot be expected. However, strong stable fibers are uniquely determined in nonlinear systems. Assuming $1 \in R_{\mathrm{ED}}$ and choosing $\bar{k}$ such that $1 \in R_{\bar{k}}$, strong stable fibers may be written for a linear system as $\mathcal{W}(j) := \bigoplus_{i=j}^{\ell+1} \mathcal{W}_n^i$, $j = \bar{k}, \ldots, \ell + 1$. In a two-dimensional system with two disjoint spectral intervals in $(0, 1)$, for example, the case $j = 1$ yields the stable fiber $\mathcal{W}(1) = \mathbb{R}^2$, while $\mathcal{W}(2)$ describes the strong stable fiber.

Uniqueness of the strong stable fiber (in black) and of the stable fiber (gray plane) is illustrated in Figure 6. Non-unique objects, like weak stable fibers are shown in green (solid and dashed curves).

The nonlinear generalization of the spaces $\mathcal{W}(j)$, $j = 1, \ldots, \ell + 1$ leads to the so called hierarchy of invariant fiber bundles. Due to [4, Theorem 4.11] and [46, Theorem 4.6.4], these bundles exist and possess a graph representation (under reasonable assumptions), describing fibers as graphs over ranges of dichotomy
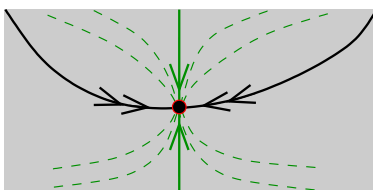
11

Figure 6: Illustration of strong and weak stable fibers in nonlinear systems.

projectors. For the latter objects, approximation results have been derived in Section 2. Based on these results, we tackle the calculation of hierarchies of fiber bundles in nonlinear systems by using a modified version of the contour algorithm from [38, 39].

In particular, we demonstrate that the contour algorithm applies to systems of dimension higher than three, allowing in this way the approximation of two- and three-dimensional projections of high-dimensional fiber bundles.

3.1 Nonlinear setup

We consider the nonlinear system (1) and assume that

(A1) $F_n \in \mathcal{C}^2(\mathbb{R}^d, \mathbb{R}^d)$ for all $n \in \mathbb{Z}$.

Denote by

$$\Psi(n, m) := \begin{cases} F_{n-1} \circ \cdots \circ F_m, & \text{for } n > m, \\ I, & \text{for } n = m \end{cases}$$

the corresponding solution operator.

First we define a reference solution w.r.t. which we compute a hierarchy of fiber bundles. Since the system (1) typically does not have an n-independent fixed point, the only meaningful nonautonomous analog turns out to be a bounded trajectory $\xi_{\mathbb{Z}}$ of (1):

(A2) $\xi_{n+1} = F_n(\xi_n)$, $n \in \mathbb{Z}$ and $\sup_{n \in \mathbb{Z}} \|\xi_n\| < \infty$.

Using Taylor's expansion, we rewrite

$$F_n(x) = F_n(\xi_n) + DF_n(\xi_n)(x - \xi_n) + Q_n(x), \quad n \in \mathbb{Z}$$

and suppose that:

(A3) For each $\varepsilon > 0$ there exists a $\delta > 0$ such that $\|DQ_n(x)\| \leq \varepsilon$ for all $\|x - \xi_n\| \leq \delta$ and all $n \in \mathbb{Z}$.

We require a set-valued Lipschitz condition, see [1, Definition 1.4.5]:

(A4) On each compact set $\mathcal{K} \subset \mathbb{R}^d$ there exists a constant $L_{F,\mathcal{K}}$ such that $F_n^{-1}(x) \subset F_n^{-1}(y) + L_{F,\mathcal{K}}\|x - y\|B$ for all $x, y \in \mathcal{K}$ and all $n \in \mathbb{Z}$. Here, B denotes the unit ball in $\mathbb{R}^d$.

12

Consider the variational equation (2) along the bounded solution from (A2). Let Σ_{ED} be the Sacker-Sell spectrum of (2) and denote by $R_{\mathrm{ED}} = \bigcup_{i=1}^{\ell+1} R_i$ the resolvent set. Let $\mathcal{W}_n^i$, $i = 1 \ldots, \ell+1$ be the spectral bundles of (2) that are defined in (11). Further assume hyperbolicity, i.e.

(A5) $1 \in R_{\mathrm{ED}}$.

We transform the bounded trajectory $\xi_{\mathbb{Z}}$ to zero and rectify subspaces via a kinematic transformation. Let

$$S_n := \left(\mathcal{B}(\mathcal{W}_n^{\ell+1}), \mathcal{B}(\mathcal{W}_n^{\ell}), \ldots, \mathcal{B}(\mathcal{W}_n^1) \right),$$

where $\mathcal{B}(\mathcal{W}_n^i)$ denotes a basis of $\mathcal{W}_n^i$. The transformed system is given as

$$x_{n+1} = G_n(x_n), \quad G_n(x) := S_{n+1}^{-1}(F_n(S_n x + \xi_n) - \xi_{n+1}), \quad n \in \mathbb{Z}. \qquad (27)$$

If $F_{\mathbb{Z}}$ satisfies (A1), (A3)–(A5) w.r.t. the bounded solution $\xi_{\mathbb{Z}}$, then $G_{\mathbb{Z}}$ satisfies these assumptions w.r.t. the zero trajectory $x_{\mathbb{Z}} = 0_{\mathbb{Z}}$. Note that (A4) holds for $G_{\mathbb{Z}}$ with a slightly modified Lipschitz constant $L_{G,\mathcal{K}}$.

By construction, G_n satisfies for $n \in \mathbb{Z}$

$$G_n(0) = 0, \quad DG_n(0) = \begin{pmatrix} A_n^{\ell+1} & & & \\ & A_n^{\ell} & & \\ & & \ddots & \\ & & & A_n^1 \end{pmatrix}, \quad A_n^i \in \mathbb{R}^{c_i,c_i}, \quad c_i = \dim(\mathcal{W}_n^i).$$

Note that the upper index of the matrices $A_{\mathbb{Z}}^i$ indicates their stability properties from strongly stable ($i = \ell+1$) to strongly unstable ($i = 1$). The rectified system (27) is introduced for simplicity of presentation only. Our algorithm applies to the original system (1); the kinematic transformation is never computed numerically.

Denote by $d_i^{s,u}$, $i = 1, \ldots, \ell+1$ the dimension of the stable respectively unstable dichotomy projector in the i-th resolvent interval R_i, see (7). We get for $k = 1, \ldots, \ell+1$ and all $n \in \mathbb{Z}$

$$G_n(x) = \begin{pmatrix} G_n^{\ell+1,k}(x) \\ G_n^{k-1,1}(x) \end{pmatrix} = \begin{pmatrix} A_n^{\ell+1,k} & 0 \\ 0 & A_n^{k-1,1} \end{pmatrix} x + \begin{pmatrix} g_n^{\ell+1,k}(x) \\ g_n^{k-1,1}(x) \end{pmatrix},$$

where $G_n^{\ell+1,k}, g_n^{\ell+1,k} \in \mathcal{C}^2(\mathbb{R}^d, \mathbb{R}^{d_k^s})$, $G_n^{k-1,1}, g_n^{k-1,1} \in \mathcal{C}^2(\mathbb{R}^d, \mathbb{R}^{d_k^u})$ and

$$A_n^{\ell+1,k} = \begin{pmatrix} A_n^{\ell+1} & & \\ & \ddots & \\ & & A_n^k \end{pmatrix} \quad A_n^{k-1,1} = \begin{pmatrix} A_n^{k-1} & & \\ & \ddots & \\ & & A_n^1 \end{pmatrix}.$$

We conclude that $g_n^{\ell+1,k}(0) = 0$, $g_n^{k-1,1}(0) = 0$, $Dg_n^{\ell+1,k}(0) = 0$ and $Dg_n^{k-1,1}(0) = 0$.

Let $\Phi^{\ell+1,k}$ and $\Phi^{k-1,1}$ be the solution operators of

$$u_{n+1} = A_n^{\ell+1,k} u_n \quad \text{and} \quad v_{n+1} = A_n^{k-1,1} v_n$$

13

and recall that the Sacker-Sell spectrum of the corresponding variational equation is invariant w.r.t. the kinematic transformation (27). The construction of $\mathcal{W}_n^i$ yields that A_n^i is invertible for all $i = 1, \ldots, \ell$, but $A_n^{\ell+1}$ might be singular. We deduce for all $n \geq m$ that

$$\|\Phi^{\ell+1,k}(n,m)\| \leq K\mathrm{e}^{-\beta_k^s(n-m)}, \quad \|\Phi^{k-1,1}(m,n)\| \leq K\mathrm{e}^{-\beta_k^u(n-m)} \qquad (28)$$

with dichotomy constants $-\beta_k^s < \beta_k^u$. The exponential rates $\beta_k^{s,u}$ belong to the unscaled variational equation (2) and they may be negative. By considering the scaled equation (6) with $\gamma \in R_k$, we obtain an exponential dichotomy with rates $\alpha_k^{s,u}$ that have, due to (23), the form

$$-\alpha_k^s = -\beta_k^s - \log\gamma < 0 < \beta_k^u - \log\gamma = \alpha_k^u.$$

3.2 Stable hierarchy of invariant fiber bundles

We define a hierarchy of locally invariant fibers under the assumptions (A1)–(A5). For simplicity, we start with the transformed system (27). By [4, Theorem 4.11] and [46, Theorem 4.6.4] there exists a hierarchy of invariant fiber bundles that are given for $k = 1, \ldots, \ell + 1$ and $n \in \mathbb{Z}$ as

$$\mathcal{L}_n^k := \left\{ \begin{pmatrix} y \\ h_n^k(y) \end{pmatrix} : y \in \mathbb{R}^{d_k^s} \cap U, \ h_n^k \in \mathcal{C}^1(\mathbb{R}^{d_k^s}, \mathbb{R}^{d_k^u}), \ h_n^k(0) = 0, \ Dh_n^k(0) = 0 \right\}.$$

These fiber bundles are locally invariant in the following sense. Let $y = \begin{pmatrix} x \\ h_n^k(x) \end{pmatrix}$ for $x \in \mathbb{R}^{d_k^s} \cap U$, $n \in \mathbb{Z}$, where U is a sufficiently small neighborhood of 0. If $G_n(y) \in U$ then

$$G_n(y) = \begin{pmatrix} G_n^{\ell+1,k}(y) \\ h_{n+1}^k(G_n^{\ell+1,k}(y)) \end{pmatrix}.$$

Furthermore, $\mathcal{L}_n^k$ is a nested sequence of locally invariant fiber bundles

$$\{0\} \subset \mathcal{L}_n^{\ell+1} \subset \mathcal{L}_n^\ell \subset \cdots \subset \mathcal{L}_n^1 = \mathbb{R}^d, \quad n \in \mathbb{Z}.$$

Assuming (A5), there exists an index $1 \leq \bar{k} \leq \ell + 1$ such that $1 \in R_{\bar{k}}$. Then $\mathcal{L}_n^{\bar{k}}$ denotes the stable n-fiber of (27) and

$$\{0\} \subset \mathcal{L}_n^{\ell+1} \subset \mathcal{L}_n^\ell \subset \cdots \subset \mathcal{L}_n^{\bar{k}}, \quad n \in \mathbb{Z}$$

defines the hierarchy of local stable fibers.

Returning to the original system (1), the hierarchy of locally invariant fibers reads for $k = 1, \ldots, \ell + 1$ and $n \in \mathbb{Z}$

$$\begin{aligned} \mathcal{L}_n^k &= \{\xi_n + x_s + h_n^k(x_s) : x_s \in \mathcal{R}(P_{k,n}^s) \cap U, \\ & \quad h_n^k \in \mathcal{C}^1(\mathcal{R}(P_{k,n}^s), \mathcal{R}(P_{k,n}^u)), \ h_n^k(0) = 0, \ Dh_n^k(0) = 0\}, \end{aligned} \qquad (29)$$

14

where U denotes a sufficiently small neighborhood of 0. Let $U_n = U + \xi_n$ for $n \in \mathbb{Z}$. We introduce a global continuation of the local stable fibers (29) for $k = \bar{k}, \ldots, \ell + 1$

$$\mathcal{H}_n^k = \left\{ x \in \mathbb{R}^d : \exists p \in \mathbb{N} : \Psi(n+i, n)x \in U_{n+i} \forall i \geq p, \ \Psi(n+p, n)x \in \mathcal{L}_{n+p}^k \right\}. \quad (30)$$

Finally, the global stable hierarchy is given by the nested sequence

$$\{0\} \subset \mathcal{H}_n^{\ell+1} \subset \mathcal{H}_n^\ell \subset \cdots \subset \mathcal{H}_n^{\bar{k}}, \quad n \in \mathbb{Z}. \quad (31)$$

In autonomous systems, this hierarchy ranges from the strong stable to the stable manifolds. We refer to [51, Chapter 5, Appendix III] in case the reference object is a fixed point of a diffeomorphism. For autonomous models, lower indices in (31) are skipped, since these sets are time independent.

3.3 Approximation of bounded trajectories

Before we start with the computation of fiber bundles, an accurate approximation on a interval $[n_-, n_+]$ of the reference object, i.e. the bounded trajectory $\xi_\mathbb{Z}$ from (A2) is needed. For this task, we choose a buffer interval $[m_-, m_+]$, where $m_- < n_- < n_+ < m_+$. Then, we solve the periodic boundary value problem

$$\begin{aligned}
x_{n+1} &= F_n(x_n), \quad n = m_-, \ldots, m_+ - 1, \\
x_{m_-} &= x_{m_+}
\end{aligned}$$

using Newton's method. Note that due to its sparse structure, the linear system that occurs in each Newton step is efficiently solvable.

It follows from (A5) that the variational equation (2) has an ED on $\mathbb{Z}$. Exploiting this hyperbolicity condition yields that any fixed tolerance Δ is reached on $[n_-, n_+]$, if the buffer interval $[m_-, m_+]$ is sufficiently large, see [37, Theorem 8]. We neglect the influence of this small error on the output of the contour algorithm in the following sections.

3.4 Approximation results for stable hierarchies

In practical applications, the graph representation of $\mathcal{L}_n^k$ is typically not explicitly given. We approximate stable fiber via the following sets:

$$\begin{aligned}
\mathcal{Z}_n^k(m, p) &= \left\{ x \in \mathbb{R}^d : (\Psi(n+m+p, n)x)_{|\mathcal{R}(P_{n+m+p,k}^u)} = 0 \right\}, \\
\mathcal{S}_n^k(m, p) &= \left\{ x \in \mathcal{Z}_n^k(m, p) : \Psi(n+i, n)x \in U_{n+i} \forall i \geq p \right\},
\end{aligned} \quad (32)$$

where $U_\mathbb{Z}$ is a sufficiently small neighborhood of $\xi_\mathbb{Z}$. These sets are nested

$$\{0\} \subset \mathcal{Z}_n^{\ell+1}(m, p) \subset \mathcal{Z}_n^\ell(m, p) \subset \cdots \subset \mathcal{Z}_n^{\bar{k}}(m, p) \subset \cdots \subset \mathcal{Z}_n^1(m, p), \quad (33)$$

$$\{0\} \subset \mathcal{S}_n^{\ell+1}(m, p) \subset \mathcal{S}_n^\ell(m, p) \subset \cdots \subset \mathcal{S}_n^{\bar{k}}(m, p)$$

for all $m, p \in \mathbb{N}$ and all $n \in \mathbb{Z}$.

Along the lines of [38, Theorem 3.3] we conclude upper-semicontinuity w.r.t. the Hausdorff semi-distance $\text{dist}(A, B) = \sup_{a \in A} \inf_{b \in B} \|a - b\|$.

15

Theorem 3 *Assume (A1)–(A5) and fix $k \geq \bar{k}$. Denote by $\beta_k^{s,u}$ the dichotomy rates w.r.t. the resolvent interval R_k, cf. (28). For any $-\beta_k^s < -\tilde{\beta}_k^s < \tilde{\beta}_k^u < \beta_k^u$ there exist a neighborhood $U_{\mathbb{Z}}$ of $\xi_{\mathbb{Z}}$, a $C > 0$ and $\omega \in \mathbb{R}$ such that*

$$\text{dist}(\mathcal{S}_n^k(m,p), \mathcal{H}_n^k) \leq C e^{\omega p} e^{-(\tilde{\beta}_k^s + \tilde{\beta}_k^u)m} \quad \text{for all } n \in \mathbb{Z} \text{ and all } m, p \in \mathbb{N}. \quad (34)$$

Unless the graph representation $\mathcal{L}_n^k$ is global for all n, it is essential for the proof of Theorem 3 and for defining (30) that starting points from $\mathcal{H}_n^k$ converge forward in time towards the bounded trajectory $\xi_{\mathbb{Z}}$. This convergence holds true if and only if $k \geq \bar{k}$ and consequently, the approximation result cannot be extended to unstable fibers.

The parameter m in (32) controls the number of steps inside the neighborhood $U_{\mathbb{Z}}$. Using the estimate (34), we conclude that all elements of $\mathcal{S}_n^k(m,p)$ lie arbitrarily close to $\mathcal{H}_n^k$, if p is fixed and m is chosen to be large.

The parameter p in (32) controls the number of steps outside the neighborhood $U_{\mathbb{Z}}$ and thus determines the length of the computed fiber. Outside the local neighborhood $U_{\mathbb{Z}}$, convergence cannot be concluded and errors may grow at most at an exponential rate, resulting in the term $e^{\omega p}$ in (34). However, an increase of m compensates for this divergent behavior.

3.5 Core of the algorithm

Our ansatz for the approximation of invariant fiber bundles is based on computing the set $\mathcal{S}_n^k(m,p)$ numerically. The core of this approach is the calculation of the set $\mathcal{Z}_n^k(m,p)$, i.e. of the kernel of $P_{n+m+p,k}^u \circ \Psi(n+m+p, n)$. Thus, one first has to determine dichotomy projectors, for which good algorithms are available as described in Section 2.5.

The second task is the detection of the zero-contour. It turns out that standard tools like Newton's method and pseudo arclength continuation for finding and continuing zeros of $P_{n+m+p,k}^u \circ \Psi(n+m+p, n)$ are hardly applicable. This is due to the fact that a large number $(m+p)$ of iteration steps, results in extremely steep gradients. Further difficulties occur, if fiber bundles have the form of several components that in addition may intersect. Various noninvertible examples show these characteristics. Finding seed points in each component – as starting points for a numerical continuation – is a nontrivial task.

We avoid these problems by using contour algorithms in MATLAB that are based on the mean-value theorem. They apply to functions $f : \mathbb{R}^r \to \mathbb{R}$, where $r \in \{2, 3\}$. Their application requires the evaluation of $f(x)$ for $x \in \Gamma$, where $\Gamma \subset \mathbb{R}^r$ is a grid in some compact area of interest. The resulting discrete data are used for detecting zero-contours. More precisely, the MATLAB command `contour` approximates zero-curves in case $r = 2$ and for $r = 3$, `isosurface` computes zero-surfaces.

Note that $\mathcal{S}_n^k(m,p) \subset \mathcal{Z}_n^k(m,p)$ and thus, one additionally has to verify for $x \in \mathcal{Z}_n^k(m,p)$, whether $\Psi(n+i, n)x \in U_{n+i}$ for $i \geq p$. Fortunately, this extra test can be neglected in several applications, see the discussion in [39, Section 3.1].

In the next sections, we overcome the restriction that the proposed method applies to two- and three-dimensional models, only. Furthermore, we introduce an extended version, allowing the calculation of hierarchies of stable fiber bundles.

3.6 Application to higher-dimensional problems

For higher-dimensional mappings $f : \mathbb{R}^r \to \mathbb{R}$, zero-hyper-surfaces are difficult to illustrate and their approximation turns out to be rather expensive due to the curse of dimension. As we will see, the intersection of this hyper-surface with an s-dimensional subspace can be visualized easily for $s = 2$, $r \geq 2$ and for $s = 3$, $r \geq 3$. Setting $s = r$ results in cases that have been discussed in Section 3.5.

3.6.1 The Lorenz manifold in a two-dimensional subspace

We illustrate this idea for $s = \{2, 3\}$, $r = 3$ by computing the Lorenz manifold, i.e. the stable manifold of the fixed point 0 of the Lorenz system, cf. [43]

$$\begin{pmatrix} x_1 \\ x_2 \\ x_3 \end{pmatrix}' = G \begin{pmatrix} x_1 \\ x_2 \\ x_3 \end{pmatrix} := \begin{pmatrix} \sigma(x_2 - x_1) \\ \varrho x_1 - x_2 - x_1 x_3 \\ x_1 x_2 - \beta x_3 \end{pmatrix}, \quad \text{with} \quad \sigma = 10, \ \varrho = 28, \ \beta = \frac{8}{3}. \tag{35}$$

Let Ψ be the solution operator of a discretization of (35) with the classical Runge-Kutta scheme of order 4 and step size $h = 0.02$. The fixed point 0 has two stable and one unstable eigenvalue. Stable dichotomy projectors in the resolvent interval R_2 possess the stable respectively unstable subspace of $DG(0)$ as range and kernel. For $s = 3$ we define $f(x) = (\Psi(m, 0)x)_{|\mathcal{R}(P^u_{m,2})}$. The left diagram in Figure 7 shows the zero-surface for $m = 100$ that we compute, using the MATLAB command `isosurface`. The right diagram shows an approximation of
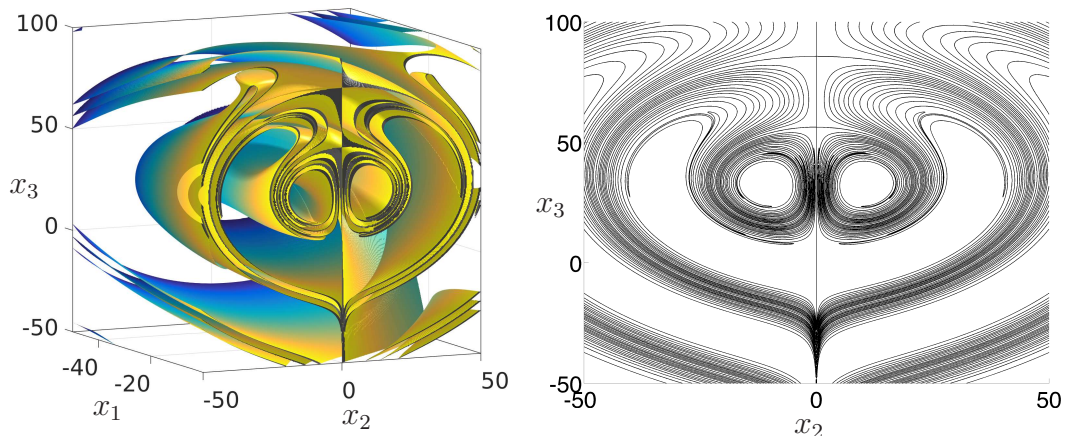

Figure 7: Approximation of the Lorenz manifold (left) and of its intersection with the (x_2, x_3) plane (right).

the intersection of the Lorenz manifold with the (x_2, x_3)-plane in high resolution.

This task corresponds to the case $s = 2$ and we define the function $f : \mathbb{R}^2 \to \mathbb{R}$ as

$$f \begin{pmatrix} x_1 \\ x_2 \end{pmatrix} = \left(\Psi(m,0) \begin{pmatrix} 0 \\ x_1 \\ x_2 \end{pmatrix} \right)_{|\mathcal{R}(P_{m,2}^u)} .$$

The zero-contour in Figure 7 (right) is calculated with $m = 200$ iteration steps of each grid point and by applying the MATLAB command `contour`. For generating Figure 7, we use a $400 \times 400 \times 400$ respectively a 2000×2000 grid.

3.6.2 A four-dimensional map

Our second example is a four-dimensional autonomous model with an explicitly given three-dimensional stable manifold:

$$F \begin{pmatrix} x_1 \\ x_2 \\ x_3 \\ x_4 \end{pmatrix} = \begin{pmatrix} \lambda_1 x_1 \\ \lambda_1 x_2 \\ \lambda_1 x_3 \\ (\lambda_1 - \lambda_2)x_1 + (\lambda_1^2 - \lambda_2)x_2^2 + (\lambda_1^3 - \lambda_2)x_3^3 + \lambda_2 x_4 \end{pmatrix} \tag{36}$$

with $0 < \lambda_1 < 1 < \lambda_2$. Here, $\{\lambda_1, \lambda_2\}$ defines the Sacker-Sell spectrum w.r.t. the fixed point $\xi = 0$. In this example, the stable subspace is not aligned to the coordinate axes and we obtain the graph representation of the stable manifold, see (29), as

$$\mathcal{H}^2 = \left\{ \begin{pmatrix} x_1 \\ x_2 \\ x_3 \\ x_1 \end{pmatrix} + h^2 \begin{pmatrix} x_1 \\ x_2 \\ x_3 \\ x_1 \end{pmatrix} : \begin{pmatrix} x_1 \\ x_2 \\ x_3 \end{pmatrix} \in \mathbb{R}^3 \right\}, \text{ where } h^2 \begin{pmatrix} x_1 \\ x_2 \\ x_3 \\ x_1 \end{pmatrix} = \begin{pmatrix} 0 \\ 0 \\ 0 \\ x_2^2 + x_3^3 \end{pmatrix}.$$

Fix $\lambda_1 = \frac{1}{2}$, $\lambda_2 = 2$. We consider the case $s = 3$, $r = 4$ and calculate in Figure 8 intersections of $\mathcal{H}^2$ with cubes Q_3, Q_2, Q_1, respectively, where $Q_i = \{x \in [-2,2]^4 : x_i = 0\}$. The case $s = 2$, $r = 4$ is shown in Figure 9 by intersecting $\mathcal{H}^2$ with selected coordinate planes. All diagrams are computed with the algorithm
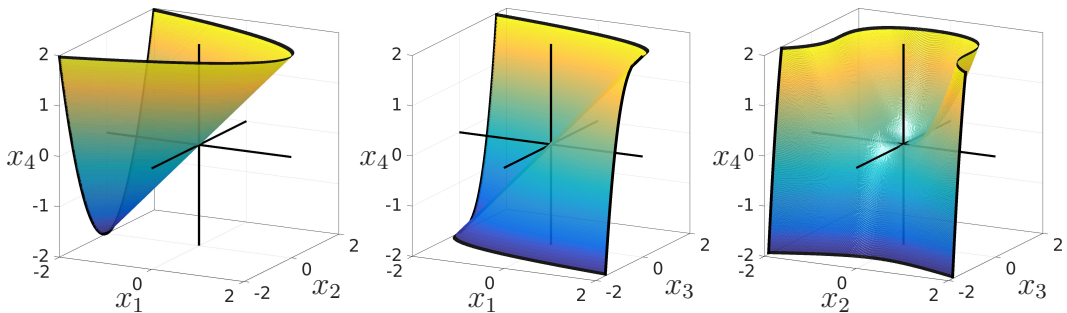

Figure 8: Intersection of the stable manifold of (36) with three-dimensional cubes.

from Section 3.5. Each point from a $400 \times 400 \times 400$ respectively 2000×2000 grid is expanded into $\mathbb{R}^4$ and then iterated for $m = 20$ steps.
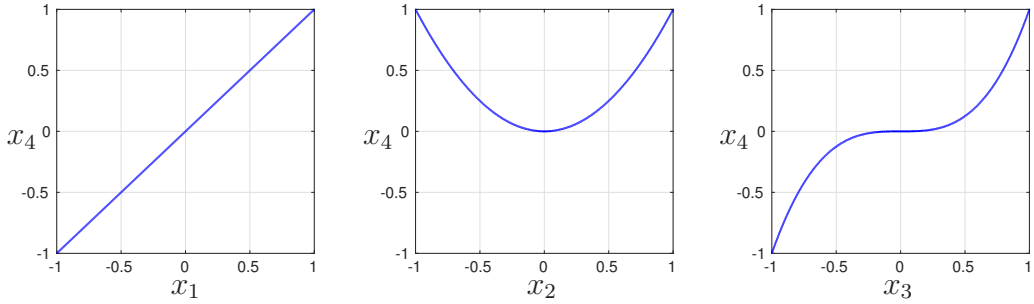
Figure 9: Intersection of the stable manifold of (36) with two-dimensional coordinate planes.

3.7 Computing hierarchies of stable fibers

In the previous sections, the calculation of zero-contours of mappings $f : \mathbb{R}^r \to \mathbb{R}$ has been considered. Standard tools like the MATLAB commands `contour` and `isosurface` solve this problem in case $r = 2$ and $r = 3$, respectively. For higher-dimensional systems, we discussed in Section 3.6 the computation of two- and three-dimensional projections.

Approximation techniques for hierarchies of stable fibers require the calculation of zero-contours of mappings $f : \mathbb{R}^r \to \mathbb{R}^j$ for $j = 1, \ldots, r-1$. These contours are nested and the case $j = 1$ is efficiently solvable. Calculating these contours one by one results in an algorithm for computing the whole stable hierarchy. Note that efficient software is currently not available for the direct computation of contours and isosurfaces of $f : \mathbb{R}^{m+j} \to \mathbb{R}^m$ if $m \geq 2$ and $j \in \{1, 2\}$.

The ranks of two consecutive projectors from (8) may vary by more than one. In this case, we artificially insert further projectors into the sequence (8). This results in a new nested sequence of projectors for $n \in \mathbb{Z}$

$$\mathbb{R}^d = \mathcal{R}(\tilde{P}^u_{n,d+1}) \supset \mathcal{R}(\tilde{P}^u_{n,d}) \supset \cdots \supset \mathcal{R}(\tilde{P}^u_{n,1}) = \{0\}$$

having the following properties:

$$\mathcal{R}(I - \tilde{P}^u_{n,j+1}) \subset \mathcal{R}(I - \tilde{P}^u_{n,j}), \quad \text{for } j = 1, \ldots, d,$$
$$\operatorname{rank}(\tilde{P}^u_{n,j}) = j - 1, \quad \text{for } j = 1, \ldots, d+1,$$
$$P^u_{n,k} = \tilde{P}^u_{n,\zeta(k)}, \quad \text{for } k = 1, \ldots, \ell+1 \text{ with } \zeta(k) = \operatorname{rank}(P^u_{n,k}) + 1.$$

In case $d = \ell$ we obtain $\tilde{P}^u_{n,j} = P^u_{n,j}$ and the rank of these projectors equals $j - 1$ as required.

We define for $j = 1, \ldots, d+1$ the family of functions

$$f_j(x) = (\Psi(n + m + p, n)x)_{|\mathcal{R}(\tilde{P}^u_{n+m+p,j})} \tag{37}$$

as well as their zero-contours

$$\mathcal{N}_j = \{x \in \mathbb{R}^d : f_j(x) = 0\}$$

19

that are nested, cf. (33).

Note that $\mathcal{N}_1 = \mathbb{R}^d$ and $\mathcal{N}_2$ is the zero-contour of $f_2 : \mathbb{R}^d \to \mathbb{R}$. Inductively, we proceed as follows. Assume that $\mathcal{N}_j$ has already been computed. This set describes a $d-j+1$-dimensional hyperplane in $\mathbb{R}^d$. Let $g_j : \mathbb{R}^{d-j+1} \cap V_j \to \mathbb{R}^d$ be a local parametrization of $\mathcal{N}_j$ in a sufficiently small neighborhood $V_j \subset \mathbb{R}^{d-j+1}$. In our applications, we find the parametrization g_j via numerical interpolation. Using $\mathcal{R}(\tilde{P}^u_{n,j+1}) \cap \mathcal{R}(I - \tilde{P}^u_{n,j}) = \mathcal{R}(\tilde{P}^u_{n,j+1} - \tilde{P}^u_{n,j})$, we conclude that

$$\mathcal{N}_{j+1} \supset \{g_j(y) : y \in \mathbb{R}^{d-j+1} \cap V_j, f_{j,j+1}(g_j(y)) = 0\}, \tag{38}$$

where $f_{j,j+1}(x) := (\Psi(n+m+p, n)x)_{|\mathcal{R}(\tilde{P}^u_{n+m+p,j+1} - \tilde{P}^u_{n+m+p,j})}$. This set is numerically accessible, since $f_{j,j+1} \circ g_j : \mathbb{R}^{d-j+1} \to \mathbb{R}$. In higher-dimensional models, we apply the approach from Section 3.6 throughout these computations.

In a nutshell, the nested sequence

$$\{0\} = \mathcal{N}_d \subset \mathcal{N}_{d-1} \subset \cdots \subset \mathcal{N}_1 = \mathbb{R}^d$$

is numerically accessible. By construction,

$$\mathcal{N}_{\zeta(k)} = \mathcal{Z}_n^k(m,p) \quad \text{for all} \quad k = 1, \ldots, \ell+1$$

and $\mathcal{Z}_n^k(m,p)$ respectively $\mathcal{S}_n^k(m,p)$ (see the discussion at the end of Section 3.5) approximate the stable fiber $\mathcal{H}_n^k$ for $k \geq \bar{k}$ thanks to Theorem 3. Thus, the sets $N_{\zeta(k)}, k = \bar{k}, \ldots, \ell+1$ establish the desired approximation of the stable hierarchy.

3.8 Three examples with explicitly given hierarchies

For an illustration of the numerical procedure from Section 3.7, we construct three autonomous models in $\mathbb{R}^3$ with explicitly given hierarchies w.r.t. the fixed point 0. The first one is invertible and has a three-dimensional stable manifold, i.e. $\bar{k} = 1$, with $\bar{k}$ from Section 3.2. In the second model, $\bar{k} = 2$ and the Jacobian at the fixed point has a zero-eigenvalue. The third model possesses a two-dimensional unstable manifold, i.e. $\bar{k} = 3$.

3.8.1 An invertible system with $\bar{k} = 1$

We consider the system

$$x_{n+1} = F(x_n), \quad n \in \mathbb{Z}, \quad \text{where} \quad F\begin{pmatrix} x_1 \\ x_2 \\ x_3 \end{pmatrix} = \begin{pmatrix} \frac{1}{4}x_1 \\ \frac{1}{2}x_1 + \frac{1}{2}x_2 \\ -\frac{11}{16}x_1^2 - \frac{1}{4}x_2 + \frac{3}{4}x_3 \end{pmatrix}. \tag{39}$$

Since this system is autonomous, fiber bundles are invariant manifolds that do not depend on time. We aim for an approximation of the hierarchy of stable manifolds of the fixed point 0. The variational equation exhibits the Sacker-Sell spectrum $\Sigma_{\text{ED}} = \{\frac{1}{4}, \frac{1}{2}, \frac{3}{4}\}$ and the resolvent intervals are $R_1 = (\frac{3}{4}, \infty)$, $R_2 = (\frac{1}{2}, \frac{3}{4})$, $R_3 =$

$(\frac{1}{4}, \frac{1}{2})$ and $R_4 = (0, \frac{1}{4})$. Here, $\ell = 3$ and $\bar{k} = 1$. Note that the ranges of dichotomy projectors – which are eigenspaces of $DF(0)$ in this autonomous model – are not aligned to the coordinate axes. Eigenvectors w.r.t. the eigenvalues $\frac{1}{4}$, $\frac{1}{2}$, $\frac{3}{4}$ are

$$v_1 = \begin{pmatrix} 1 \\ -2 \\ -1 \end{pmatrix}, \quad v_2 = \begin{pmatrix} 0 \\ 1 \\ 1 \end{pmatrix}, \quad v_3 = \begin{pmatrix} 0 \\ 0 \\ 1 \end{pmatrix}.$$

All manifolds from the stable hierarchy have global graph representations (29) that are given as

$$
\begin{aligned}
\mathcal{H}^1 = \mathcal{L}^1 &= \mathbb{R}^3, \\
\mathcal{H}^2 = \mathcal{L}^2 &= \left\{ \lambda_1 v_1 + \lambda_2 v_2 + h^2(\lambda_1 v_1 + \lambda_2 v_2) : \begin{pmatrix} \lambda_1 \\ \lambda_2 \end{pmatrix} \in \mathbb{R}^2 \right\} \\
&\qquad \text{with} \quad h^2(\lambda_1 v_1 + \lambda_2 v_2) = \lambda_1^2 v_3, \\
\mathcal{H}^3 = \mathcal{L}^2 &= \left\{ \lambda_1 v_1 + h^3(\lambda_1 v_1) : \lambda_1 \in \mathbb{R} \right\} \quad \text{with} \quad h^3(\lambda_1 v_1) = \lambda_1^2 v_3, \\
\mathcal{H}^4 = \mathcal{L}^4 &= \{0\}.
\end{aligned}
\tag{40}
$$

These sets are nested, i.e. (31) holds. Furthermore, we find for $\mathcal{H}^2$ and $\mathcal{H}^3$ the alternative representations

$$\mathcal{H}^2 = \left\{ \begin{pmatrix} x_1 \\ x_2 \\ x_1 + x_1^2 + x_2 \end{pmatrix} : \begin{pmatrix} x_1 \\ x_2 \end{pmatrix} \in \mathbb{R}^2 \right\}, \quad \mathcal{H}^3 = \left\{ \begin{pmatrix} x_1 \\ -2x_1 \\ -x_1 + x_1^2 \end{pmatrix} : x_1 \in \mathbb{R} \right\}.$$

Computing the zero-contour $\mathcal{N}_2$ of f_2, defined in (37), we obtain an approximation of $\mathcal{H}^2$. In Figure 10 (left) we choose a $300 \times 300 \times 300$ grid and $m = 10$ iteration steps within the contour algorithm. Then, we interpolate the numerical data w.r.t. the tangent space $\mathrm{span}\{v_1, v_2\}$ and obtain $\tilde{g}_2$ as an approximation of g_2. The graph of $\tilde{g}_2$ is shown in the right panel of Figure 10.

For calculating an approximation of $\mathcal{H}^3$, we use the proposed method from Section 3.7. We choose a 2000×2000 grid in $[-4, 4] \times [-4, 4]$. Then we compute the set $\mathcal{N}_3$ as defined in (38) (right panel of Figure 10). For this task, the MATLAB command `contour` applies.

Finally, we discuss approximation errors. Starting with $\mathcal{H}^2$, we plot in the left diagram of Figure 11 pointwise errors in case $m = 10$. It turns out that an increase of m does not result in smaller errors as suggested by our error estimate (34). Observed errors are caused by linear interpolation that is used for both, computing the zero-contour and for interpolating the data to obtain $\tilde{g}_2$. As a consequence, errors are of magnitude $\mathcal{O}(\Delta^2)$, where Δ is the spacing of the grid, used for the contour algorithm.

Interestingly, the computation of $\mathcal{H}^3$ does not show this problem. Interpolation errors turn out to be negligible when calculating the zero-contour $\mathcal{N}_3^{\mathrm{proj}} := \{y \in \mathbb{R}^2 : f_{2,3}(\tilde{g}_2(y)) = 0\} \subset \mathbb{R}^2$, cf. (38). Here, it is essential not to map the resulting points onto $\mathcal{H}^2$ by computing $\mathcal{N}_3 \approx \tilde{g}_2(\mathcal{N}_3^{\mathrm{proj}})$, since this operation will
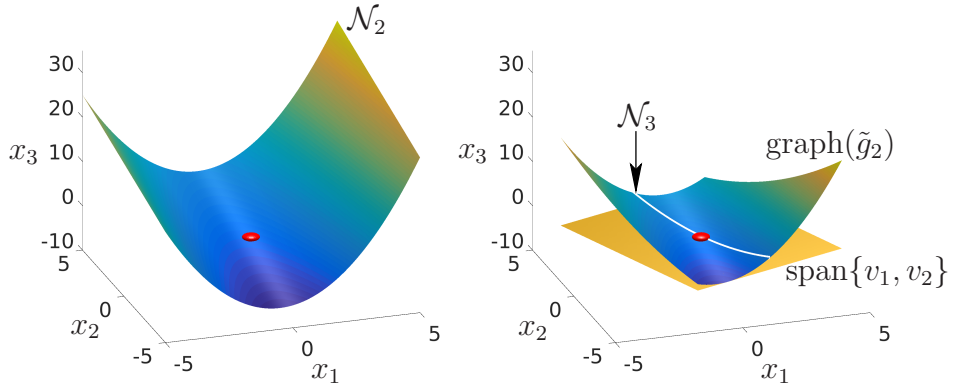
Figure 10: Approximation of $\mathcal{H}^2$ for (39) w.r.t. $\xi = 0$ (red ball). Zero-contour $\mathcal{N}_2$ (left) and interpolated graph representation $\tilde{g}_2$ w.r.t. the tangent space span$\{v_1, v_2\}$ (right). The approximate strong stable manifold $\mathcal{N}_3$ is shown in white.

reintroduce interpolation errors. Instead, we measure the error of $\mathcal{N}_3^{\text{proj}}$ in the right diagram of Figure 11. The logarithmic slope of these data is -0.6972. This supports the error estimate (34) from Theorem 3, since $-(\beta_3^s + \beta_3^u) = -(-\log(\frac{1}{4}) + \log(\frac{1}{2})) = -\log(2) \approx -0.69315$.
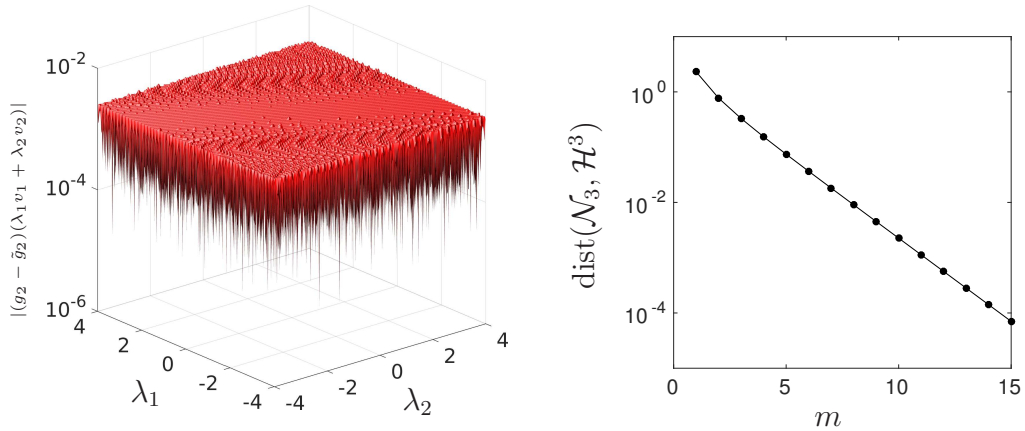
Figure 11: Approximation error of $\mathcal{N}_2$ for $m = 10$ w.r.t. the parameterization (40) (left). Distance of $\mathcal{H}^3$ to its numerical approximation for $m = 1, \ldots, 20$ (right).

3.8.2 A system with zero-eigenvalue and $\bar{k} = 2$

Dichotomy projectors within the resolvent interval $R_{\ell+1} = R_3$ are nontrivial for the next model. Note that the resolvent interval R_3 corresponds to the eigenvalue

0, see Figure 1 (lower case). We consider

$$x_{n+1} = F(x_n), \quad n \in \mathbb{Z}, \quad \text{where} \quad F\begin{pmatrix} x_1 \\ x_2 \\ x_3 \end{pmatrix} = \begin{pmatrix} 0 \\ \frac{1}{2}x_1 + \frac{1}{2}x_2 \\ \frac{1}{4}x_1^2 + \frac{1}{2}x_1 x_2 - \frac{7}{4}x_2^2 + 2x_3 \end{pmatrix}.$$
(41)

The manifolds $\mathcal{H}^2$ and $\mathcal{H}^3$ have the explicit representations

$$\mathcal{L}^2 = \mathcal{H}^2 = \left\{ \begin{pmatrix} x_1 \\ x_2 \\ x_2^2 \end{pmatrix} : \begin{pmatrix} x_1 \\ x_2 \end{pmatrix} \in \mathbb{R}^2 \right\}, \quad \mathcal{L}^3 = \mathcal{H}^3 = \left\{ \begin{pmatrix} x_1 \\ -x_1 \\ x_1^2 \end{pmatrix} : x_1 \in \mathbb{R} \right\}.$$

We numerically determine the stable manifold $\mathcal{H}^2$ as well as the strong stable manifold $\mathcal{H}^3$ as described in Section 3.8.1 and analyze approximation errors of $\mathcal{H}^3$ in Figure 12. Due to the zero-eigenvalue of $DF(0)$, we conclude that $\alpha_{\ell+1}^s = \infty$ as discussed at the end of Section 2.6. As a consequence, we expect from (34) that no (relevant) errors occur, when calculating $\mathcal{H}^3$ numerically. This confirms the error plot in Figure 12.
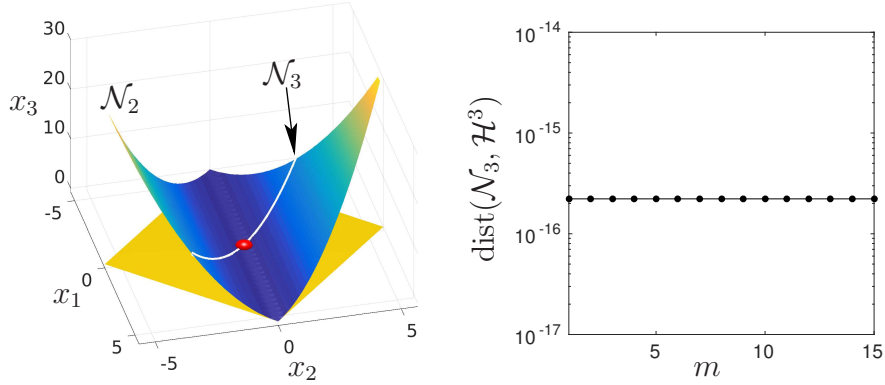

Figure 12: Approximation of $\mathcal{H}^2$ and $\mathcal{H}^3$ for (41) (left) and distance of $\mathcal{H}^3$ to its approximation w.r.t. $m = 1, \ldots, 15$ (right).

3.8.3 A system with $\bar{k} = 3$

The next model illustrates that one-dimensional stable manifolds in three-dimensional systems are numerically accessible. Let

$$x_{n+1} = F(x_n), \quad n \in \mathbb{Z}, \quad \text{where} \quad F\begin{pmatrix} x_1 \\ x_2 \\ x_3 \end{pmatrix} = \begin{pmatrix} \frac{1}{2}x_1 \\ x_1 + 2x_2 \\ -\frac{11}{4}x_1^2 + 3x_3 \end{pmatrix}. \quad (42)$$

The fiber $\mathcal{L}^2$ and the stable manifold $\mathcal{H}^3$ have the explicit representations

$$\mathcal{L}^2 = \left\{ \begin{pmatrix} x_1 \\ x_2 \\ x_1^2 \end{pmatrix} : \begin{pmatrix} x_1 \\ x_2 \end{pmatrix} \in \mathbb{R}^2 \right\}, \quad \mathcal{H}^3 = \mathcal{L}^3 = \left\{ \begin{pmatrix} -3x_1 \\ 2x_1 \\ 9x_1^2 \end{pmatrix} : x_1 \in \mathbb{R} \right\}.$$

23

We apply the contour algorithm as described in Section 3.8.1 for obtaining approximations of $\mathcal{L}^2$ and $\mathcal{H}^3$ in Figure 13. Here, it is important to note that the graph representation of $\mathcal{L}^2$ contains a weak unstable manifold, which is not unique. By considering this weak unstable manifold as a quasibounded trajectory forward in time, see [4, Definition 3.1], one can establish uniqueness, at least for a cutoff version of (42), cf. [48, Proposition 3.3]. Theorem 3 justifies the approximation of $\mathcal{H}^3$, and the numerical experiment in Figure 13 (left) indicates that nevertheless $\mathcal{N}_2 \approx \mathcal{L}^2$.

Due to (34), the exponential rate of convergence of $\mathcal{H}^3$ depends on the dichotomy rates w.r.t. the resolvent interval $R_3 = (\frac{1}{2}, 2)$: $-(\beta_3^s + \beta_3^u) = -2\log 2 \approx -1.386294$. This coincides with the numerical data in Figure 13 (right), having the exponential slope -1.386483.
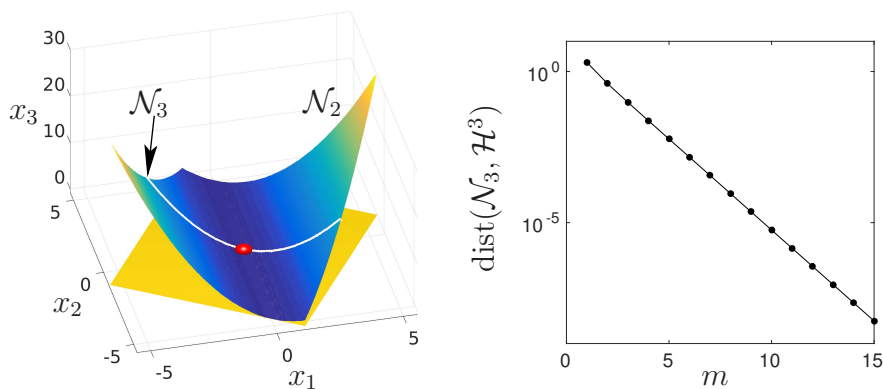

Figure 13: Approximation of $\mathcal{L}^2$ and $\mathcal{H}^3$ for (42) (left) and distance of $\mathcal{H}^3$ to its approximation w.r.t. $m = 1, \ldots, 15$ (right).

3.9 An noninvertible example

We consider the noninvertible autonomous system

$$x_{n+1} = F(x_n), \quad n \in \mathbb{Z}, \quad \text{where} \quad F\begin{pmatrix} x_1 \\ x_2 \\ x_3 \end{pmatrix} = \begin{pmatrix} \frac{1}{4}x_1 + x_3^2 \\ \frac{1}{2}x_2 - x_1 x_2 \\ 2x_3 + x_2^2 \end{pmatrix}. \qquad (43)$$

The stable manifold $\mathcal{H}^2$ of the fixed point 0 does not possess a global graph representation, see Figure 16. For its calculation, we apply the contour algorithm on a $400 \times 400 \times 400$ grid in $[-4, 4] \times [-2, 2] \times [-2, 0.5]$ and iterate each grid point for 6 steps.

Next, we aim for an approximation of the strong stable manifold $\mathcal{H}^3$. The calculation of (38) requires local parametrizations of $\mathcal{H}^2$. For constructing them, we first compute the primary part of $\mathcal{H}^2$, using a cutoff version of F

$$\begin{aligned} \tilde{F}(x) &= DF(0)x + \chi(\mu\|x\|)(F(x) - DF(0)x), \\ \chi(z) &= \max\{\min\{2 - z, 1\}, 0\}. \end{aligned} \qquad (44)$$

24

The resulting function exhibits almost global parametrizations. We parametrize x_3 as a function of $x_1 \in [-4, 4]$ and $x_2 \in [-0.2, 0.2]$ in the left of Figure 14. The right diagram shows a parametrization of x_2 as a function of $x_1 \in [-4, 4]$ and $x_3 \in [-2, 0]$.
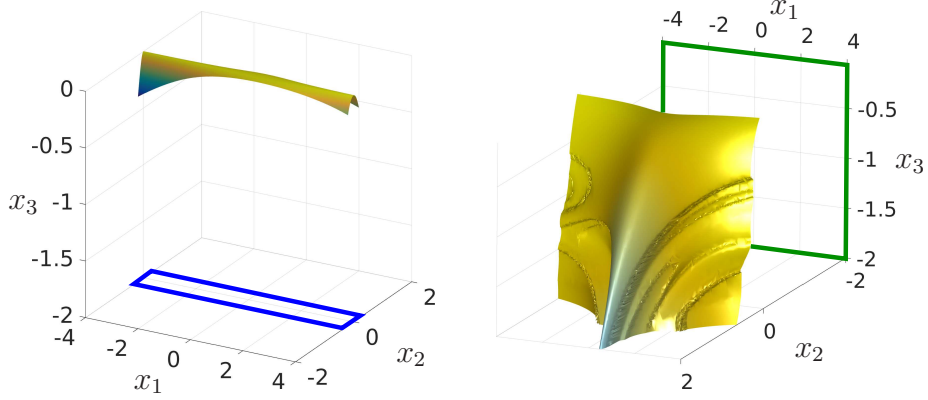

Figure 14: Parametrizations of $\mathcal{H}^2$, computed using the cutoff function (44) with $\mu = \frac{1}{4}$.

With respect to these parametrizations, we determine zero-contours as proposed in (38). Carrying out the contour algorithm, each point on a 2000×2000 grid in the blue respectively green rectangle from Figure 14 is mapped to $\mathcal{H}^2$, using the corresponding parametrization. Then these points are iterated for 4 steps. The resulting data are used to compute the zero-contours in Figure 15.

These contours are mapped to $\mathcal{H}^2$ in Figure 16. Exploiting the symmetry property

$$F \begin{pmatrix} x_1 \\ -x_2 \\ x_3 \end{pmatrix} = \begin{pmatrix} F_1 \\ -F_2 \\ F_3 \end{pmatrix} \begin{pmatrix} x_1 \\ x_2 \\ x_3 \end{pmatrix},$$

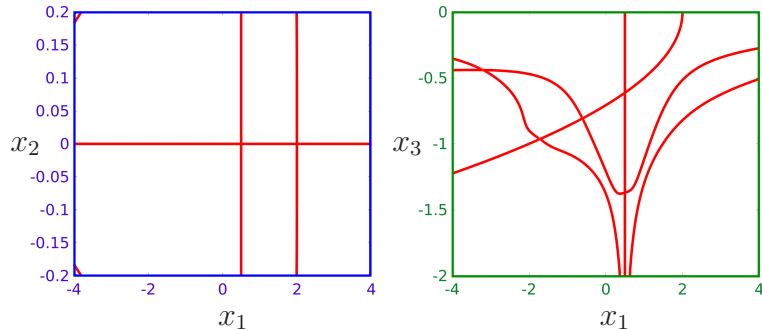we obtain data for both, positive and negative values of x_2 from the right contour in Figure 15.

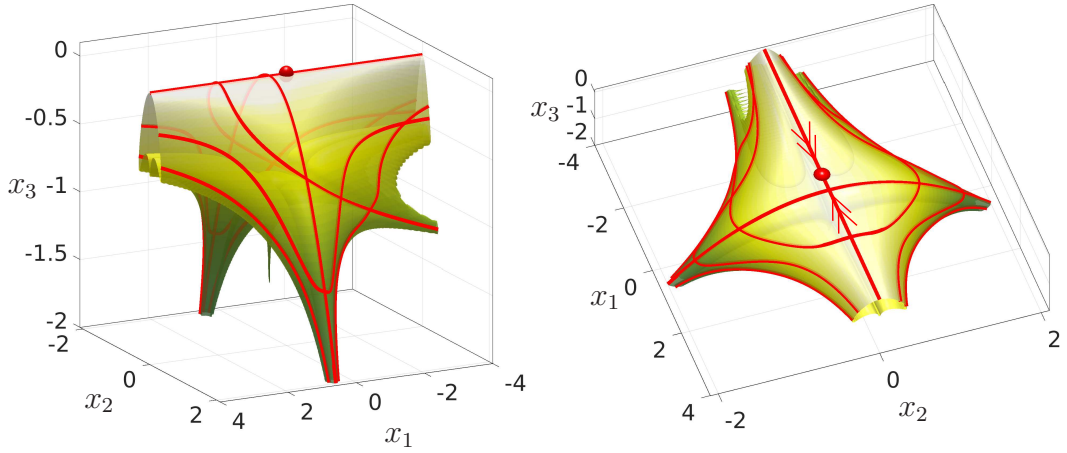Figure 15: Zero-contours (38) w.r.t. the parametrizations from Figure 14.

25

Figure 16: Approximation of the stable manifold $\mathcal{H}^2$ of (43) w.r.t. the fixed point 0 (red ball). The red lines are parts of the strong stable manifold $\mathcal{H}^3$.

Finally, we observe that $\mathcal{H}^3 \supset \mathcal{H}^{3,1} \cup \mathcal{H}^{3,2}$, where

$$
\mathcal{H}^{3,1} := \left\{ \begin{pmatrix} \eta \\ 0 \\ 0 \end{pmatrix} : \eta \in \mathbb{R} \right\}, \quad \mathcal{H}^{3,2} := \left\{ \begin{pmatrix} \frac{1}{2} \\ \eta \\ -\frac{1}{2}\eta^2 \end{pmatrix} : \eta \in \mathbb{R} \right\},
$$

since all elements from $\mathcal{H}^{3,1}$ converge to 0 with the exponential rate $\log\frac{1}{4}$ and $F(x) \in \mathcal{H}^{3,1}$ for all $x \in \mathcal{H}^{3,2}$, see Figure 17. Note that Figure 16 contains further parts of the strong stable manifold that are mapped to $\mathcal{H}^{3,2}$.

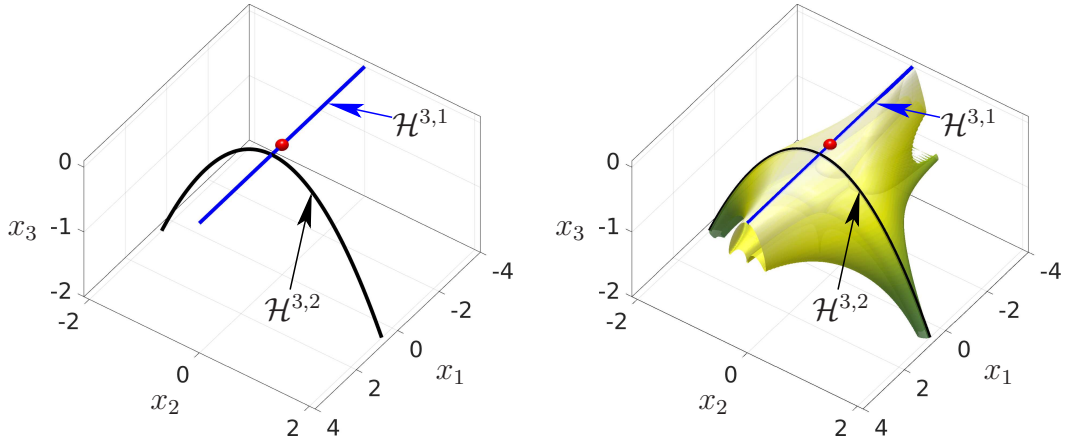
Figure 17: Illustration of parts of the strong stable manifold of the fixed point 0.

3.10 The nonautonomous Lorenz system

Our final example is a nonautonomous generalization of the Lorenz system

$$\begin{pmatrix} x_1 \\ x_2 \\ x_3 \end{pmatrix}' = \begin{pmatrix} \sigma(x_2 - x_1) \\ \varrho x_1 - x_2 - x_1 x_3 \\ x_1 x_2 - \beta(t) x_3 \end{pmatrix}, \quad \sigma = 10, \quad \varrho = 28, \quad \beta(t) = \tfrac{4}{3}(1 + e^{-t}). \quad (45)$$

To this ODE-model, we apply the classical Runge-Kutta scheme of order 4 with step size 0.02. Approximations of the stable fiber bundle $\mathcal{H}_t^2$ of the fixed point 0 are computed on a $300 \times 300 \times 300$ grid in $[-30, 30]^3$. The contour algorithm iterates each grid point for 100 Runge-Kutta steps.

For finding an approximation of the strong stable fiber $\mathcal{H}_t^3$, we proceed as in Section 3.9 and calculate the principle part of the stable fiber using cutoff techniques. Then, we evaluate (38), map the resulting contours to the approximation of $\mathcal{H}_t^2$ and obtain the hierarchy of fiber bundles, shown in Figures 18, 19. In Figure 20, we recompute the fibers $\mathcal{H}_0^2$ and $\mathcal{H}_0^3$ on a larger domain.
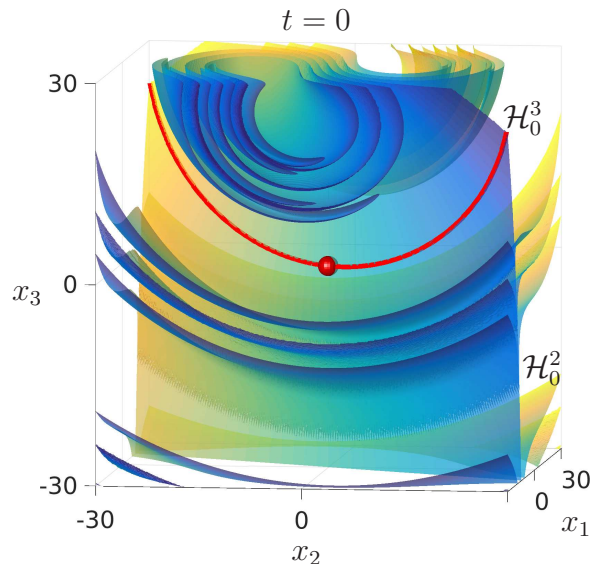

Figure 18: Approximation of the stable and strong stable fiber (in red) of the fixed point 0 (red ball) for the nonautonomous Lorenz system (45) at time $t = 0$.
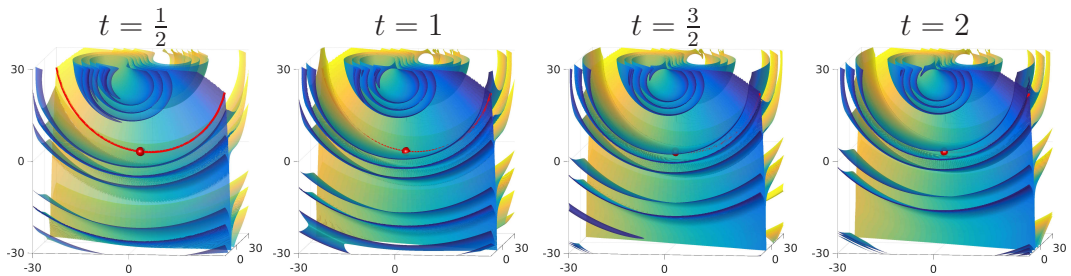
Figure 19: Approximation of the stable and strong stable fiber of the fixed point 0 (red ball) for the nonautonomous Lorenz system (45) at times $t \in \{\frac{1}{2}, 1, \frac{3}{2}, 2\}$. In the right diagrams, the strong stable manifold is hidden by parts of the stable manifold.
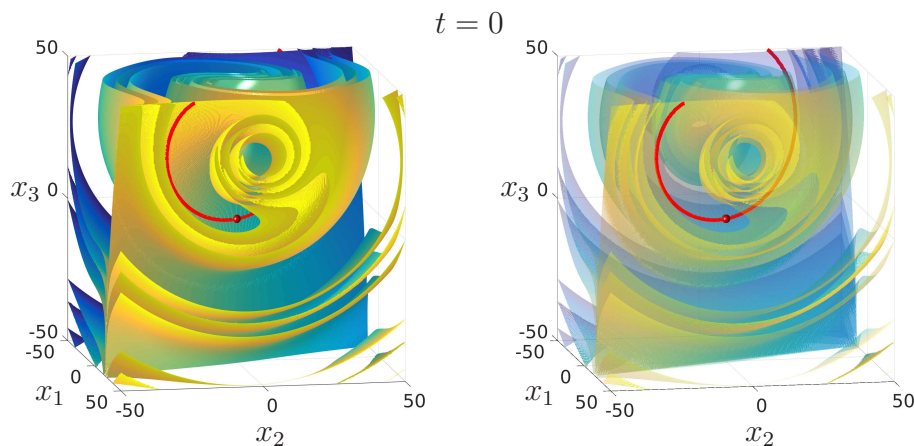

Figure 20: Approximation of the stable fiber (left: solid, right: transparent) and of the strong stable fiber (in red) of the fixed point 0 for the nonautonomous Lorenz system (45) at time $t = 0$.

4 Conclusion

The appropriate spectral concept for nonautonomous linear systems turns out to be the Sacker-Sell spectrum. Dichotomy projectors and thus, spectral bundles are numerically accessible. Corresponding methods and error estimates are given, including their proofs.

Appropriate reference objects for nonlinear systems are bounded trajectories and we aim for an approximation of their stable hierarchies. The proposed variant of the contour algorithm solves this task by computing fibers from the hierarchy one after another. In principle, restrictions on the dimension of the system and on the dimension of the stable fiber are not required.

If the system (1) is invertible, then our approach also applies to the inverted system

$$x_{n+1} = F_n^{-1}(x_n), \quad n \in \mathbb{Z} \tag{46}$$

and provides the stable hierarchy of (46), which is the unstable hierarchy of the original system (1).

Hierarchies of fiber bundles for ODE models can be computed by applying our method to a time h-map that we obtain, for example, using a one-step discretization scheme. In particular, a negative step size results in an approximation of the unstable hierarchy.

It is an interesting problem to consider the difference equation (1) on a finite time interval only, resulting in a finite time dynamical system. Corresponding linear and nonlinear results as well as finite time versions of invariant fibers have been developed, see for example [7, 6, 21, 29, 30, 31]. However, fibers in finite time are fat objects. One may interpret approximations that are computed with the contour algorithm as parts of fat finite time fibers. But it is still an open question whether the whole finite time object is accessible in this way.

Acknowledgment

References

[1] J.-P. Aubin and H. Frankowska. *Set-valued analysis*. Modern Birkhäuser Classics. Birkhäuser Boston, Inc., Boston, MA, 2009.

[2] B. Aulbach. The fundamental existence theorem on invariant fiber bundles. *J. Differ. Equations Appl.*, 3(5-6):501–537, 1998.

[3] B. Aulbach and J. Kalkbrenner. Exponential forward splitting for noninvertible difference equations. *Comput. Math. Appl.*, 42(3-5):743–754, 2001.

[4] B. Aulbach, C. Pötzsche, and S. Siegmund. A smoothness theorem for invariant fiber bundles. *J. Dynam. Differential Equations*, 14(3):519–547, 2002.

[5] B. Aulbach and S. Siegmund. The dichotomy spectrum for noninvertible systems of linear difference equations. *J. Differ. Equations Appl.*, 7(6):895–913, 2001.

[6] A. Berger, T. S. Doan, and S. Siegmund. A definition of spectrum for differential equations on finite time. *J. Differential Equations*, 246(3):1098–1118, 2009.

[7] A. Berger, D. T. Son, and S. Siegmund. Nonautonomous finite-time dynamics. *Discrete Contin. Dyn. Syst. Ser. B*, 9(3-4):463–492, 2008.

[8] W.-J. Beyn and W. Kleß. Numerical Taylor expansions of invariant manifolds in large dynamical systems. *Numer. Math.*, 80(1):1–38, 1998.

[9] D. Blazevski and J. Franklin. Using scattering theory to compute invariant manifolds and numerical results for the laser-driven Hénon-Heiles system. *Chaos*, 22(4):043138, 9, 2012.

[10] X. Cabré, E. Fontich, and R. de la Llave. The parameterization method for invariant manifolds. III. Overview and applications. *J. Differential Equations*, 218(2):444–515, 2005.

[11] M. Canadell and R. de la Llave. KAM tori and whiskered invariant tori for non-autonomous systems. *Phys. D*, 310:104–113, 2015.

[12] M. J. Capiński and C. Simó. Computer assisted proof for normally hyperbolic invariant manifolds. *Nonlinearity*, 25(7):1997–2026, 2012.

[13] M. J. Capiński and P. Zgliczyński. Geometric proof for normally hyperbolic invariant manifolds. *J. Differential Equations*, 259(11):6215–6286, 2015.

[14] F. Colonius and W. Kliemann. *The dynamics of control.* Systems & Control: Foundations & Applications. Birkhäuser Boston, Inc., Boston, MA, 2000.

[15] W. A. Coppel. *Dichotomies in Stability Theory.* Springer, Berlin, 1978. Lecture Notes in Mathematics, Vol. 629.

[16] J. L. Daleckiĭ and M. G. Kreĭn. *Stability of Solutions of Differential Equations in Banach Space.* American Mathematical Society, Providence, R.I., 1974.

[17] M. Dellnitz and A. Hohmann. A subdivision algorithm for the computation of unstable manifolds and global attractors. *Numer. Math.*, 75(3):293–317, 1997.

[18] L. Dieci, C. Elia, and E. Van Vleck. Exponential dichotomy on the real line: SVD and QR methods. *J. Differential Equations*, 248(2):287–308, 2010.

[19] L. Dieci and E. S. Van Vleck. Lyapunov and Sacker-Sell spectral intervals. *J. Dynam. Differential Equations*, 19(2):265–293, 2007.

[20] E. J. Doedel, B. Krauskopf, and H. M. Osinga. Global organization of phase space in the transition to chaos in the Lorenz system. *Nonlinearity*, 28(11):R113–R139, 2015.

[21] L. H. Duc and S. Siegmund. Hyperbolicity and invariant manifolds for planar nonautonomous systems on finite time intervals. *Internat. J. Bifur. Chaos Appl. Sci. Engrg.*, 18(3):641–674, 2008.

[22] T. Eirola and J. von Pfaler. Numerical Taylor expansions for invariant manifolds. *Numer. Math.*, 99(1):25–46, 2004.

[23] J. P. England, B. Krauskopf, and H. M. Osinga. Computing one-dimensional stable manifolds and stable sets of planar maps without the inverse. *SIAM J. Appl. Dyn. Syst.*, 3(2):161–190 (electronic), 2004.

[24] J.-L. Figueras and À. Haro. Reliable computation of robust response tori on the verge of breakdown. *SIAM J. Appl. Dyn. Syst.*, 11(2):597–628, 2012.

[25] G. Froyland, T. Hüls, G. P. Morriss, and T. M. Watson. Computing covariant Lyapunov vectors, Oseledets vectors, and dichotomy projectors: A comparative numerical study. *Phys. D*, 247:18–39, 2013.

[26] G. Froyland, S. Lloyd, and N. Santitissadeekorn. Coherent sets for nonautonomous dynamical systems. *Phys. D*, 239(16):1527–1541, 2010.

[27] A. Girod and T. Hüls. Nonautonomous systems with transversal homoclinic structures under discretization. *BIT*, 56(2):605–631, 2016.

[28] J. Hadamard. Sur l'itératio et les solutions asymptotiques des équations différentielles. *Bull. Soc. Math. France*, 29:224–228, 1901.

[29] G. Haller. Finding finite-time invariant manifolds in two-dimensional velocity fields. *Chaos*, 10(1):99–108, 2000.

[30] G. Haller. Lagrangian structures and the rate of strain in a partition of two-dimensional turbulence. *Phys. Fluids*, 13(11):3365–3385, 2001.

[31] G. Haller. Lagrangian coherent structures. *Annual Review of Fluid Mechanics*, 47:137–162, 2015.

[32] À. Haro, M. Canadell, J.-L. Figueras, A. Luque, and J.-M. Mondelo. *The parameterization method for invariant manifolds – From rigorous results to effective computations*, volume 195 of *Applied Mathematical Sciences*. Springer, 2016.

[33] D. Henry. *Geometric Theory of Semilinear Parabolic Equations*. Springer, Berlin, 1981.

[34] M. W. Hirsch, C. C. Pugh, and M. Shub. *Invariant manifolds*. Springer, Berlin, 1977. Lecture Notes in Mathematics, Vol. 583.

[35] T. Hüls. Numerical computation of dichotomy rates and projectors in discrete time. *Discrete Contin. Dyn. Syst. Ser. B*, 12(1):109–131, 2009.

[36] T. Hüls. Computing Sacker-Sell spectra in discrete time dynamical systems. *SIAM J. Numer. Anal.*, 48(6):2043–2064, 2010.

[37] T. Hüls. Homoclinic trajectories of non-autonomous maps. *J. Difference Equ. Appl.*, 17(1):9–31, 2011.

[38] T. Hüls. A contour algorithm for computing stable fiber bundles of nonautonomous, noninvertible maps. *SIAM J. Appl. Dyn. Syst.*, 15(2):923–951, 2016.

[39] T. Hüls. On the approximation of stable and unstable fiber bundles of (non)autonomous ODEs — A contour algorithm. *Internat. J. Bifur. Chaos Appl. Sci. Engrg.*, 26(7):1650118, 10, 2016.

[40] T. Hüls and C. Pötzsche. Qualitative analysis of a nonautonomous Beverton-Holt Ricker model. *SIAM J. Appl. Dyn. Syst.*, 13(4):1442–1488, 2014.

[41] J. Kalkbrenner. *Exponentielle Dichotomie und chaotische Dynamik nichtinvertierbarer Differenzengleichungen*, volume 1 of *Augsburger Mathematisch-Naturwissenschaftliche Schriften*. Dr. Bernd Wißner, Augsburg, 1994.

[42] B. Krauskopf, H. M. Osinga, E. J. Doedel, M. E. Henderson, J. Guckenheimer, A. Vladimirsky, M. Dellnitz, and O. Junge. A survey of methods for computing (un)stable manifolds of vector fields. *Internat. J. Bifur. Chaos Appl. Sci. Engrg.*, 15(3):763–791, 2005.

[43] E. N. Lorenz. Deterministic nonperiodic flow. *J. Atmos. Sci.*, 20(2):130–141, 1963.

[44] O. Perron. Die Stabilitätsfrage bei Differentialgleichungen. *Math. Z.*, 32(1):703–728, 1930.

[45] H. Poincaré. Mémoire sur les courbes défines par une équation différentielle (iv). *Journal de Mathématiques Pures et Appliquées*, 2:151–217, 1886.

[46] C. Pötzsche. *Geometric theory of discrete nonautonomous dynamical systems*, volume 2002 of *Lecture Notes in Mathematics*. Springer, Berlin, 2010.

[47] C. Pötzsche. Fine structure of the dichotomy spectrum. *Integral Equations Operator Theory*, 73(1):107–151, 2012.

[48] C. Pötzsche and M. Rasmussen. Taylor approximation of invariant fiber bundles for nonautonomous difference equations. *Nonlinear Anal.*, 60(7):1303–1330, 2005.

[49] C. Pötzsche and M. Rasmussen. Computation of nonautonomous invariant and inertial manifolds. *Numer. Math.*, 112(3):449–483, 2009.

[50] R. J. Sacker and G. R. Sell. A spectral theory for linear differential systems. *J. Differential Equations*, 27(3):320–358, 1978.

[51] M. Shub. *Global stability of dynamical systems*. Springer, New York, 1987.

[52] C. Simó. On the analytical and numerical approximation of invariant manifolds. In D. Benest and C. Froeschlé, editors, *Les méthodes modernes de la mécanique céleste*, pages 285–329. 1989.

[53] S. Wiggins. *Normally hyperbolic invariant manifolds in dynamical systems*, volume 105 of *Applied Mathematical Sciences*. Springer, New York, 1994.